Ref. Ares(2022)1998052 - 18/03/2022

Funded by European Union Civil Protection
Grant Agreement Number 874421

Vulnerability assessment of embankments and bridges exposed to flooding hazards

Deliverable D4.2

Report on Vulnerability Assessment Methodology - Fragility curves for bridges subjected to flooding

Project Information

Grant Agreement No.	874421
Project Acronym	oVERFLOw
Project Full Title	Vulnerability assessment of embankments and bridges exposed to flooding hazards
Starting Date	1 December 2019
Duration	32 months
Call Identifier	UCPM-2019-PP-AG
Topic	UCPM-2019-PP-PREV-AG: Prevention in civil protection and marine pollution
Project Website	www.projectoverflow.eu
Project Coordinator	Prof. Meho Sasa Kovacevic
Organisation	Faculty of Civil Engineering, University of Zagreb
E-mail	msk@grad.hr
Telephone	+385 (1) 4639 250

Partner Information

Sveuciliste u Zagrebu Gradevinski Fakultet	Croatia
Infra Plan Konzalting	Croatia
GEKOM - geofizikalno i ekološko modeliranje d.o.o.	Croatia
VEILIGHEIDSREGIO ZUID-HOLLAND ZUID	Netherlands
INGEO BV	Netherlands
ZAVOD ZA GRADBENISTVO SLOVENIJE	Slovenia
Uprava Republike Slovenije za zaščito in reševanje	Slovenia

Document Information

Work Package	4
Deliverable Title	Report on Vulnerability Assessment Methodology - Fragility curves for bridges subjected to flooding
Version	2.0
Date of Submission	3/15/2022
Main Editor(s)	Mirko Kosič
Contributor(s)	Mirko Kosič, Andrej Anžlin
Reviewer(s)	I.Stipanovic, K. Gavin
Citation	M. Kosič, A. Anžlin (2022). oVERFLOw Deliverable 4.2 Report on Vulnerability Assessment Methodology - Fragility curves for bridges subjected to flooding

Document Classification:									
Draft		Final	X	Confidential		Restricted		Public	X

History			
Version	**Issue Date**	**Status**	**Distribution**
1	2/28/2022	Draft for review	All partners
2	3/15/2022	Final	All partners

The information contained in this report reflects the views of the Author(s), and the Commission does not accept responsibility for the use of this information.

Executive Summary

This deliverable is a report on the vulnerability assessment of the two case study bridges, i.e. the Banija Bridge and the Karlovac Bridge. The deliverable puts forward a methodology for vulnerability analysis of bridges subjected to flooding and an advanced modelling approach for simulation of the bridge response considering soil-structure interaction. The performed study considers different flooding scenarios, including hydrodynamic loads, debris and scour. Several failure mechanisms were identified in relation to the considered flooding scenarios. The major outcomes of the deliverable are fragility surfaces for the serviceability and ultimate limit state for the two case study bridges, which will provide crucial input for the development of the risk forecasting tool within WP5 and validation activities within WP6.

Keywords: vulnerability analysis, bridges, fragility surface, numerical modelling, failure mechanism, debris, scour.

Table of Contents

Project Information ii
Partner Information ii
Document Information iii
Executive Summary iv
1 Abbreviations and Acronyms 6
2 Introduction 7
3 Case study bridges and input data for analysis 8
3.1 Banija Bridge 8
3.2 Karlovac Bridge 11
3.3 Geotechnical data 14
3.4 Hydrological data 17
3.5 Measured modal properties 18
4 Methodology for bridge vulnerability assessment 21
5 Numerical modelling approach 23
5.1 Structural modelling 24
5.2 Soil-structure interaction 25
5.3 Load modelling 28
5.4 Scour modelling 30
6 Validation of the numerical approach 32
6.1 Banija Bridge 32
6.2 Karlovac Bridge 34
7 Vulnerability analysis and results 36
7.1 Banija Bridge 37
7.2 Karlovac Bridge 45
8 Conclusions 52
9 References 54

1 Abbreviations and Acronyms

Abbreviation / Acronym	Description
CPT	CONE PENETRATION TEST
IM	INTENSITY MEASURE
LS	LIMIT STATE
ND	NOT DETECTED
RC	REINFORCED CONCRETE
SLS	SERVICEABILITY LIMIT STATE
SPT	STANDARD PENETRATION TEST
SSI	SOIL-STRUCTURE INTERACTION
UP	UTILIZATION PERCENTAGE
ULS	ULTIMATE LIMIT STATE
WP	WORK PACKAGE

2 Introduction

This deliverable is a report on the vulnerability assessment of the two case study bridges, i.e. the Banija Bridge and the Karlovac Bridge. Due to specific hydraulic conditions addressed in Deliverable 2.2 [1], it was reasonable to consider flooding hazards using two parameters, i.e. water height and flow velocity. Ergo, fragility surfaces instead of fragility curves need to be developed. The main goal of this document is, therefore, to establish fragility surfaces for the serviceability and ultimate limit state. They represent the probability of exceeding the designated limit states for a given combination of water height and flow velocity. The fragility surfaces will provide crucial input for developing the risk forecasting tool within WP5 and validation activities within WP6.

In the first part of the deliverable, two bridges from the case study area City of Karlovac are presented along with the available data for the analysis. Following this introductory part, the deliverable puts forward a methodology for vulnerability analysis of bridges subjected to flooding and an advanced modelling approach for simulation of the bridge response considering soil-structure interaction. The study considers different flood-loading scenarios, including hydrodynamic loads, debris and scour. Special attention is devoted to the explicit simulation of the effect of scouring on the distribution of forces in the structure. Several failure mechanisms are considered, and the most unfavourable mechanism for the given flooding scenario is identified.

Before the vulnerability analysis, the modelling approach used to analyse the case study bridges is validated against the results of ambient vibration measurements. The vulnerability analysis is performed separately for the serviceability and ultimate limit state. Since both velocity and water height were found to be necessary for precise estimation of the bridge performance, the result of the vulnerability analysis is presented with fragility surfaces, which represent an extension of the classical fragility curve concept.

The deliverable concludes with a summary of the most important findings.

3 Case study bridges and input data for analysis

In this chapter, two bridges analysed in the case study area city of Karlovac are presented (see Figure 1), with the most relevant data for the vulnerability analysis, such as geotechnical data and hydrological data measured bridge modal parameters.

Figure 1: Case study area of the City of Karlovac with the representation of the two case study bridges [2].

3.1 Banija Bridge

The Banija Bridge is a steel-riveted girder bridge built between 1945 and 1947 (Figure 2). After World War II, the bridge was rebuilt when the older bridge from 1889 was demolished. The original construction plans of the bridge are not available. The input data for the analysis was obtained from a retrofitting project from 2017([3], [4]), which was complemented with results of a drone and bathymetric survey, and ambient vibration measurements documented in Deliverable D3.2 [5]. The results of the drone and bathymetric surveys were used to define the geometry, whereas measurements of ambient vibration allow the estimation of the bridge's modal properties.

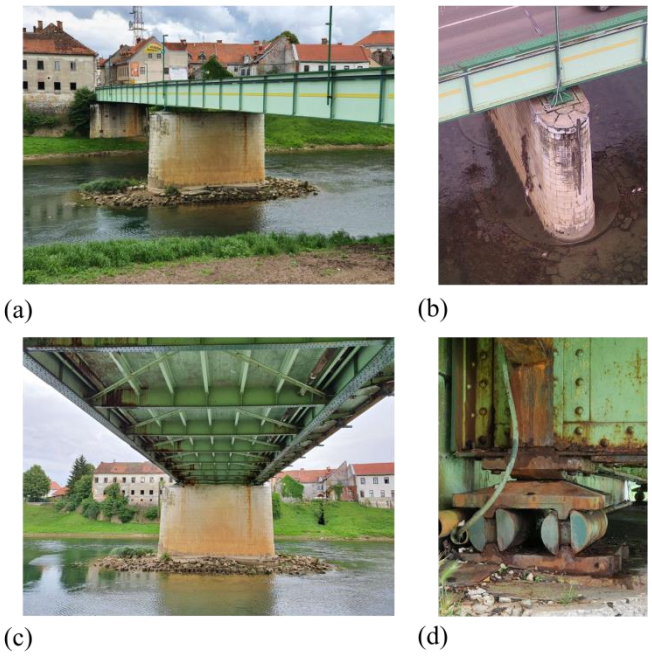

Figure 2: Overview of the Banija Bridge: (a) Side view, (b) Detail of the middle pier and well foundations, (c) View below the bridge deck, (d) Detail of the roller bearing at the abutment

The Banija Bridge has two main spans of length 48.6 m, with the middle pier founded in the riverbed of the Kupa River. The bridge spans a total length of 97.2 m and has a total width of 12.4 m. It supports two traffic lines and a pedestrian zone constructed on cantilever beams. The cross-section of the bridge is presented in Figure 3.

The two main girders have riveted I-shape cross-sections with varied thicknesses of the flanges to follow the bending moment line. The main girders are joined together every 4.05 m by riveted transverse beams. The transverse beams are connected with seven I-shaped stringers that support the RC slab of the deck (Figure 3).

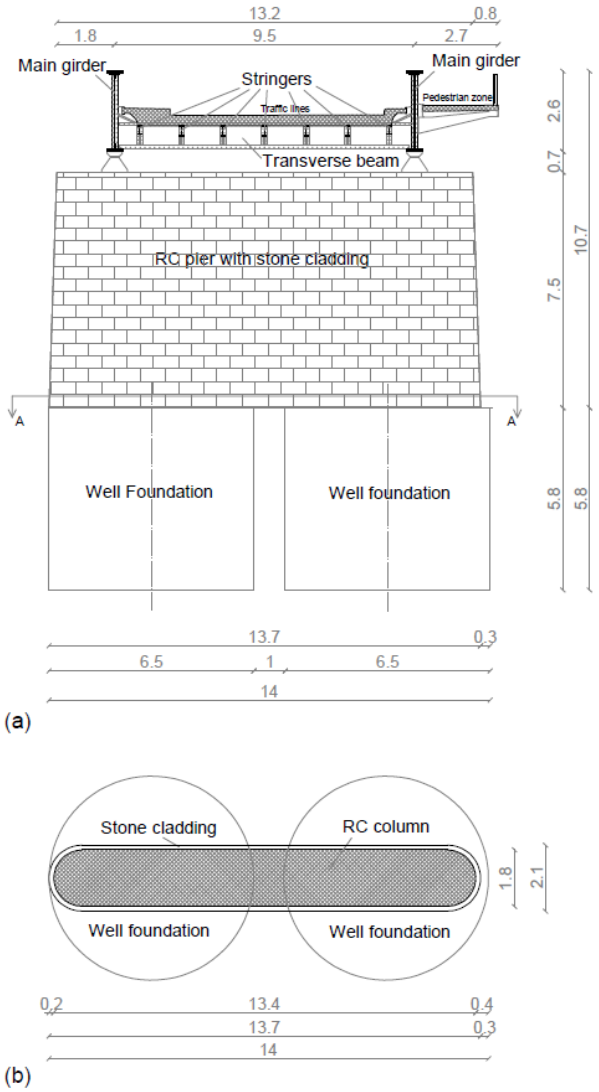

Figure 3: (a) Cross-section of the Banija Bridge in the first span, (b) Cross-section A-A at the base of the pier.

At the abutments, the bridge is supported by longitudinal roller bearings of diameter 20 cm (Figure 2d). The transverse displacement is restrained with two shear keys of dimensions 3 cm x 6 cm. Translation of the bridge at the middle pier is restrained in all directions by the use of shear pins of diameter 5 cm.

The pier and the abutments are made of RC and are covered with stone cladding. The middle pier has a rectangular section with rounded ends. The outside dimension of the pier is 13.7 x 2.1 m at the bottom and 13.2 x 2.1 m at the top. The height of the pier from the foundation level to the top is 7.5 m. The pier is founded on two large well foundations of a diameter of 6.5 m. Due to a lack of construction plans, the depth of the foundations was assumed to be equal to the one used for the old Banija Bridge from 1889 (5.8 m), for which part of historic construction plans was obtained in Croatian State Archives. The depth of the stone cladding was estimated to be equal to 15 cm. The abutments are not described herein in detail since they will not be modelled explicitly in numerical analysis.

The mechanical characteristics of the superstructure were obtained from the destructive testing performed with the retrofitting project [4]. The steel grade for the superstructure was estimated to be equivalent to S235 according to EN-1993-1-1 [6], whereas the grade of concrete of the bridge deck was estimated to be equivalent to C25/30 according to EN-1992-1-1 [7]. The data for the bridge pier and foundations was not available. As a simplification, the quality of the concrete was assumed to be the same (C25/30).

3.2 Karlovac Bridge

The Karlovac Bridge is an RC three-span road bridge that carries a heavily trafficked bypass road (Prilaz Većeslava Holjevca) over the Kupa River to the city of Karlovac (Figure 4). Search for the design documentation of the bridge was conducted in the archives of the city of Karlovac and the Croatian State Archives. However, the construction plans of the bridge could not be retrieved. Partial information regarding the geometry of the bridge was obtained from a recent bridge inspection report [8]. Due to the fact that this report was obtained after the submission of deliverable D3.2, some additional details regarding the geometry and materials of the bridge are provided herein.

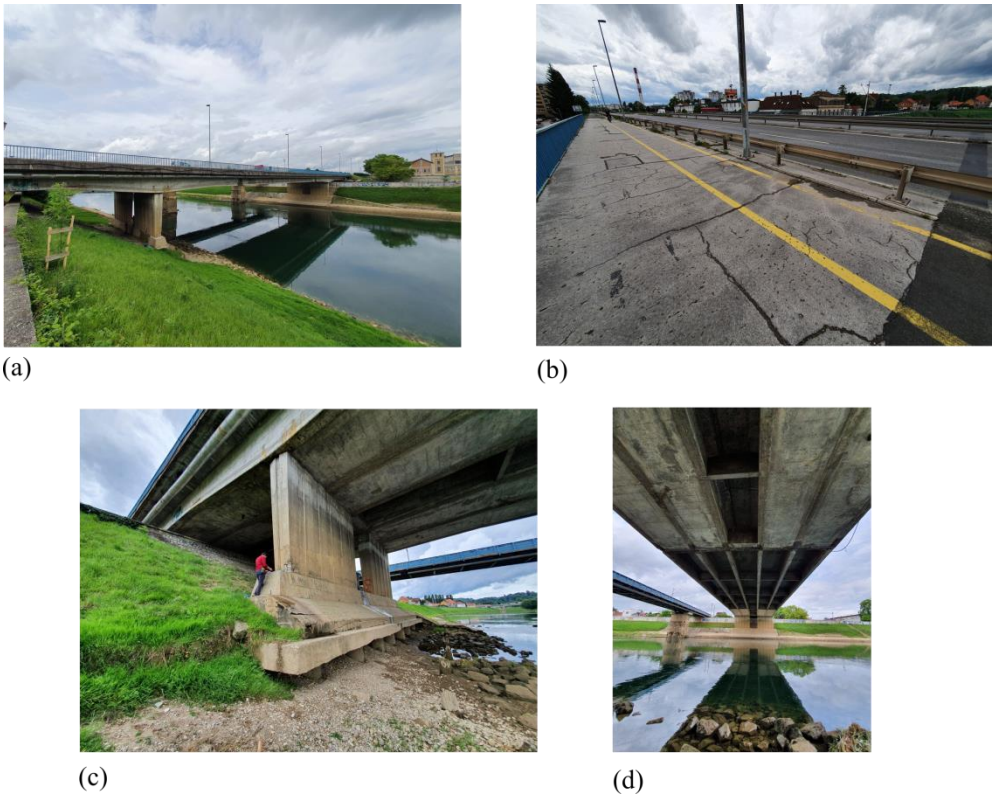

Figure 4: Overview of the Karlovac Bridge: (a) side view, (b) view of the roadway, (c) view on the south column, (d) view from below

Considering the type of structural design, it is estimated that the Karlovac Bridge was constructed in the mid-70s. The bridge is constructed in RC and has three spans with 25.7 m, 71.9 m and 26.4 m in length (Figure 5). The total length of the bridge is 124 m. The side spans of the bridge extend

continuously over the piers in the middle span with 15.9 m long cantilever segments. At the end of these cantilevers, Gerber hinges are constructed to support the middle 40 m long segment of the bridge.

The deck has a constant longitudinal inclination of 2%. The width of the bridge deck is 22 m. It holds four traffic lanes (2 in each direction) and a pedestrian zone. The traffic lanes are divided by a central reserve and are confined with sidewalks on both sides. The cross-section of the deck is composed of 6 Y-shaped prefabricated girders and a cast-in-place RC slab (Figure 6). The Y-shaped girders have a bottom width of 0.5 m and varying height between 1.75 m at the midspan and 2.5 m above the piers. The depth of the slab is estimated to be 0.5 m at the location of the traffic lines and 0.8 m elsewhere. The total height of the deck varies from 2.5 m to 3.25 m. Transverse stiffening beams are constructed in the perpendicular direction to the main beams to ensure uniform distribution of loading on all main girders.

The deck is supported by two RC piers on each side of the bridge. The piers are 5.7 m high and have a varying thickness of 1.2 m at the top and 0.8 m at the bottom. The width of the piers in the transverse direction is 7.2 m.

The piers are constructed over a continuous foundation beam with a total height of 2.9 m and a bottom width of 5.4 m. The foundation beam is supported by two lines of bored piles. Each line consists of 7 bored piles. The depth of the foundation piles could not be established based on the performed in-situ investigations. An estimate of the foundation depth was obtained based on the preliminary calculation of the bearing capacity of the pile and comparison with the applied loads. Consistent results were obtained for a pile diameter of 0.8 m and a length of 10 m. Consequently, this input data was assumed.

Due to the lack of construction plans, the materials characteristics of the concrete and reinforcing steel were unknown. The same applies to the location and amount of reinforcement. Some information regarding the quality of the material was obtained from limited destructive testing performed within the routine inspection of the bridge [8]. The measured in-situ concrete compression strengths are summarized in Table 1.

Table 1: In-situ concrete compressive strength of the Karlovac Bridge components [8]

Location	Compressive strength (MPa)
Abutment	46.2
Deck	65.7
Deck	72.6

The results in Table 1 indicate that the concrete strength of the bridge deck is larger than the concrete strength at the abutments. Consequently, concrete quality C40/50 according to EN-1992-1-1 [7] was assumed for the piers and abutments, and C50/60 for the bridge deck. Tension tests of the steel reinforcement were not performed. However, a survey of the reinforcement in the column indicated that the reinforcement is composed of smooth bars. According to the standards in place at the time of the construction, it was assumed that the tensile strength of the reinforcement was 200 MPa.

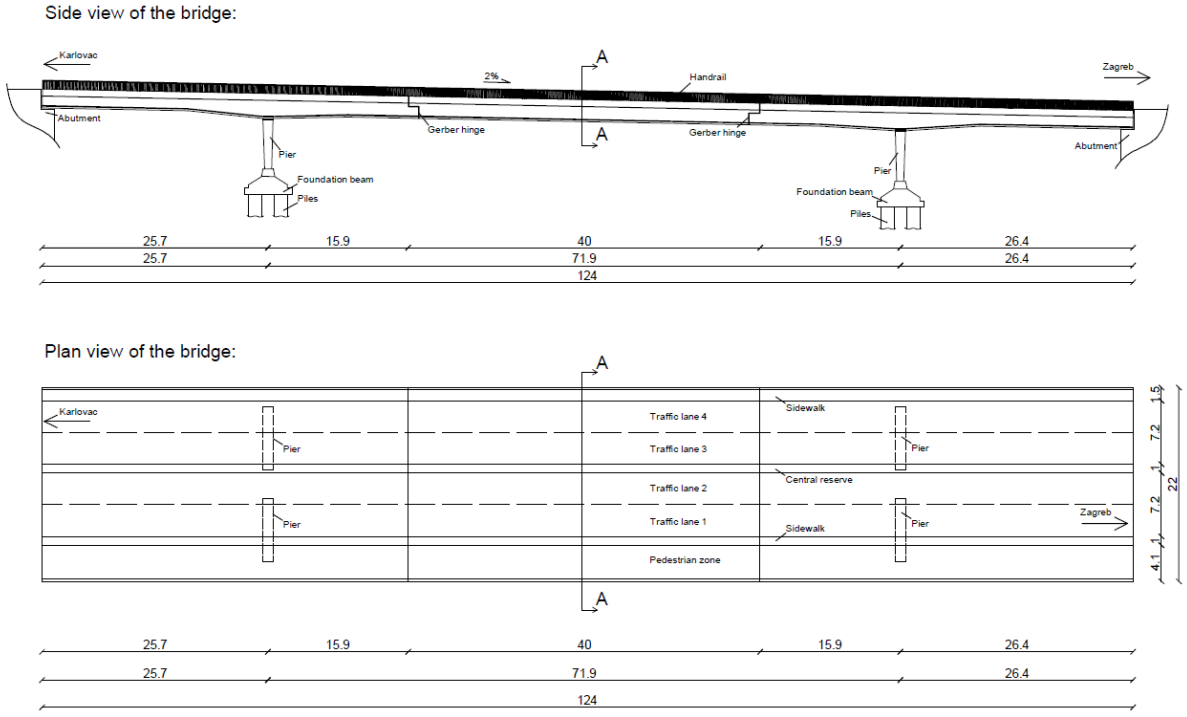

Figure 5: Side and plan view of the Karlovac Bridge

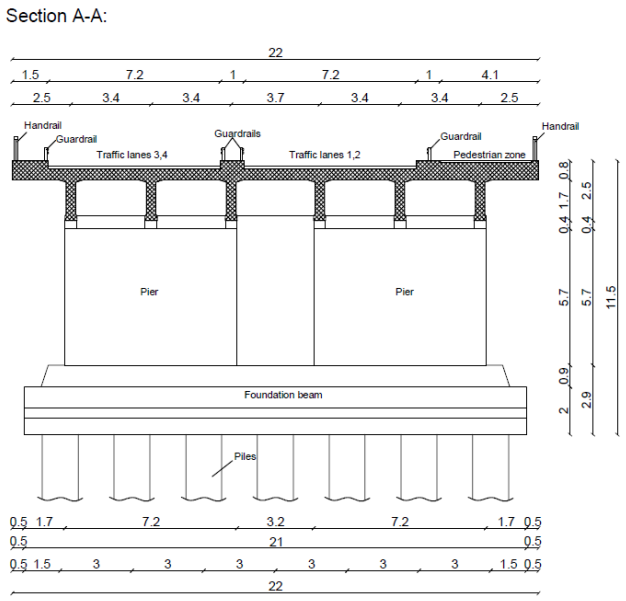

Figure 6: Cross-section A-A at the midspan of the Karlovac Bridge

3.3 Geotechnical data

In this section, geotechnical data based on the results of the CPT investigations and boreholes are presented for both bridges.

3.3.1 Banija Bridge

The geotechnical characteristics at the site of the Banija Bridge were defined from the results of CPT investigations and boreholes performed near the bridge abutments within D3.1 (see Figure 7). The soil profile was found to be composed of a top 6 meters clay layer with an underlying sand layer. Investigations performed directly near the foundations of the piers were not available. For the purpose of the modelling of the soil-structure interaction at the piers, it was assumed that the characteristics of the sand layer below the embankment are consistent with those of the sand below the foundation. Such an assumption was supported with results of geophysical investigations, which indicate that a large shear wave velocity is also present below the riverbed at a depth larger than 2 m (Figure 8). It was thus considered that the same sand layer is also presented below the foundation of the middle pier. Based on the results of Figure 7, it can be seen that the energy-corrected number of SPT blows (N_{60}) and elastic modulus (E) at the depth of the foundation (depth between 9 and 11 meters) amounted to 35 and 100 MPa, respectively.

The overburden-corrected number of SPT blows of the sand layer amount to $(N_1)_{60}$ = 25. According to empirical SPT relations, the corresponding shear angle amount to 40° degrees [9] and the relative density amount to 0.60 [10]. Based on nearby boreholes, the dry unit weight of the soil was assumed to amount to 19.8 kN/m^3. The buoyant unit weight of 9.8 kN/m^3 was thus used for modelling soil-structure interaction at the middle pier due to the fact the foundation is located in the riverbed. Due to lower overburden pressure at the foundation level of the middle pier (57 kPa), the elastic modulus from Figure 7 was reduced in accordance with the Janbu approach [11] (referenced according to [12]) to account for pressure-dependent stiffness characteristic of the soil. The estimated E at overburden pressure of 57 kPa amounted to 53 MPa. Assuming a Poisson's ratio of 0.3 for sands, the shear modulus (G) was estimated to be 19 MPa. The N_{60} was also transformed to consider lower overburden pressure. Based on $(N_1)_{60}$ = 25, the equivalent N_{60} amounted to 19. The considered soil characteristics for modelling of soil-structure interaction at the middle pier of the Banija Bridge are summarized in Table 2.

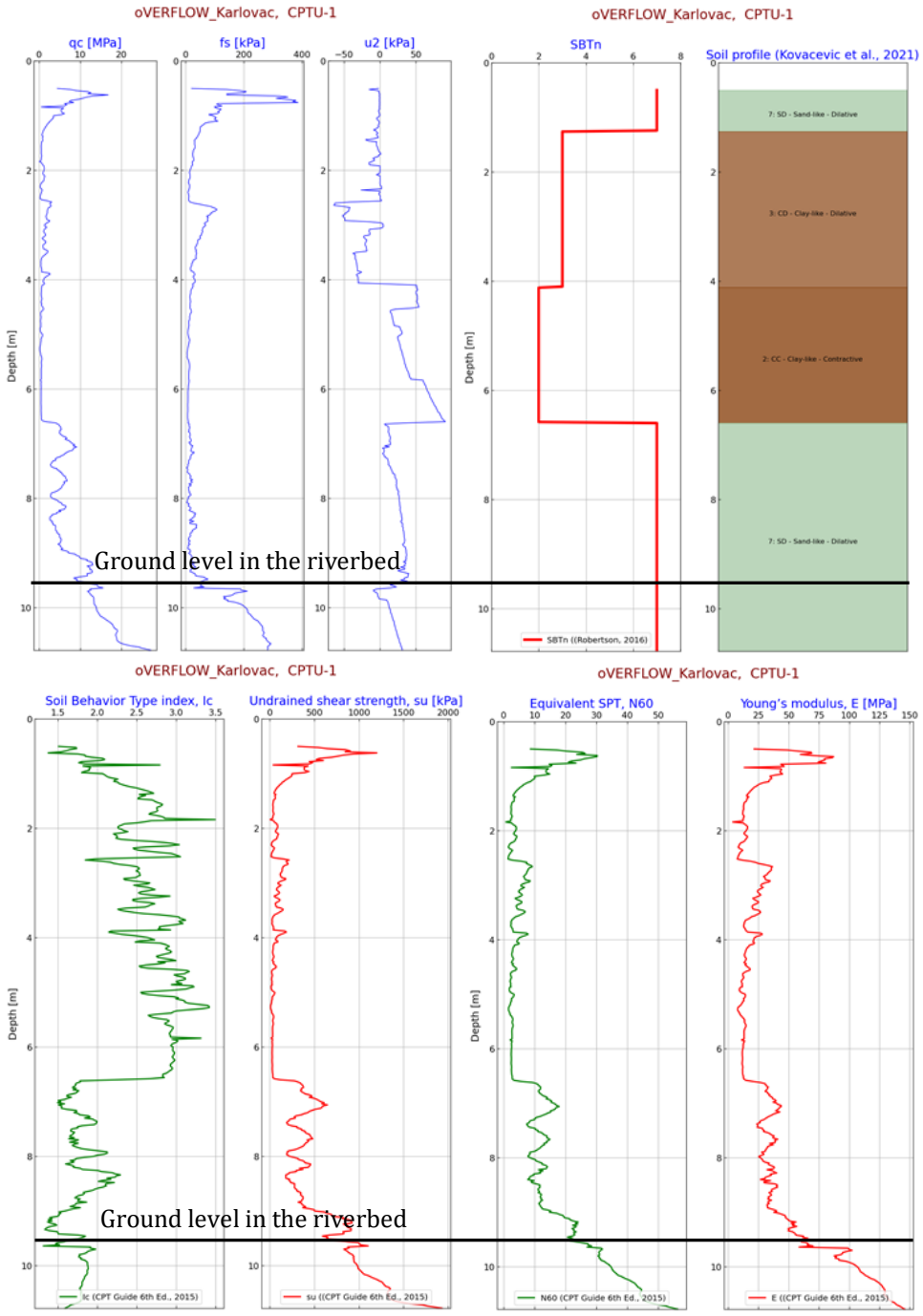

Figure 7: Results of CPTu investigation performed near the Banija Bridge abutment.

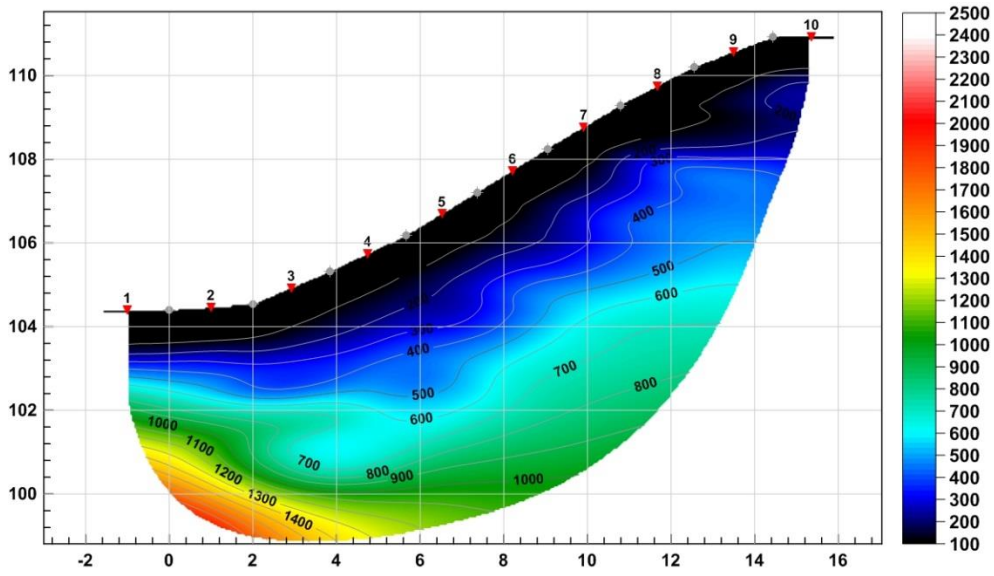

Figure 8: Soil shear wave velocity profile near the location of the Banija Bridge.

Table 2: Soil characteristics for modelling of soil-structure interaction for the Banija Bridge

Parameter	Value
Effective shear angle (φ')	40°
Effective cohesion (c')	0 kPa
Soil unit weight (γ')	19.8 kN/m3
Poisson's ratio (ν)	0.30
Elastic modulus (E)	50 Mpa
Shear modulus (G)	19 Mpa
Equivalent SPT blows (N_{60})	19

3.3.2 Karlovac Bridge

The geotechnical characteristics of the Karlovac Bridge were obtained from a borehole performed near the location of the south embankment within D3.1 (Figure 9). The borehole indicated that the soil profile is similar to the profile near the Banija Bridge, with the exception that the top layer is composed of clayey gravel instead of clay. The bottom layer is again medium dense sand. The average N_{60} in the location of the pile foundation amount to 33, which results in the overburden-corrected number of SPT blows $(N_1)_{60}$ at the mid-height of the pile foundation amount of 21. This value is very similar to the $(N_1)_{60}$ obtained for the foundation of the Banija Bridge. Considering that average overburden pressures at the location of the foundations are also similar (about 60 kPa), it was considered appropriate to consider the same geotechnical parameters as used for the Banija Bridge (see Table 2).

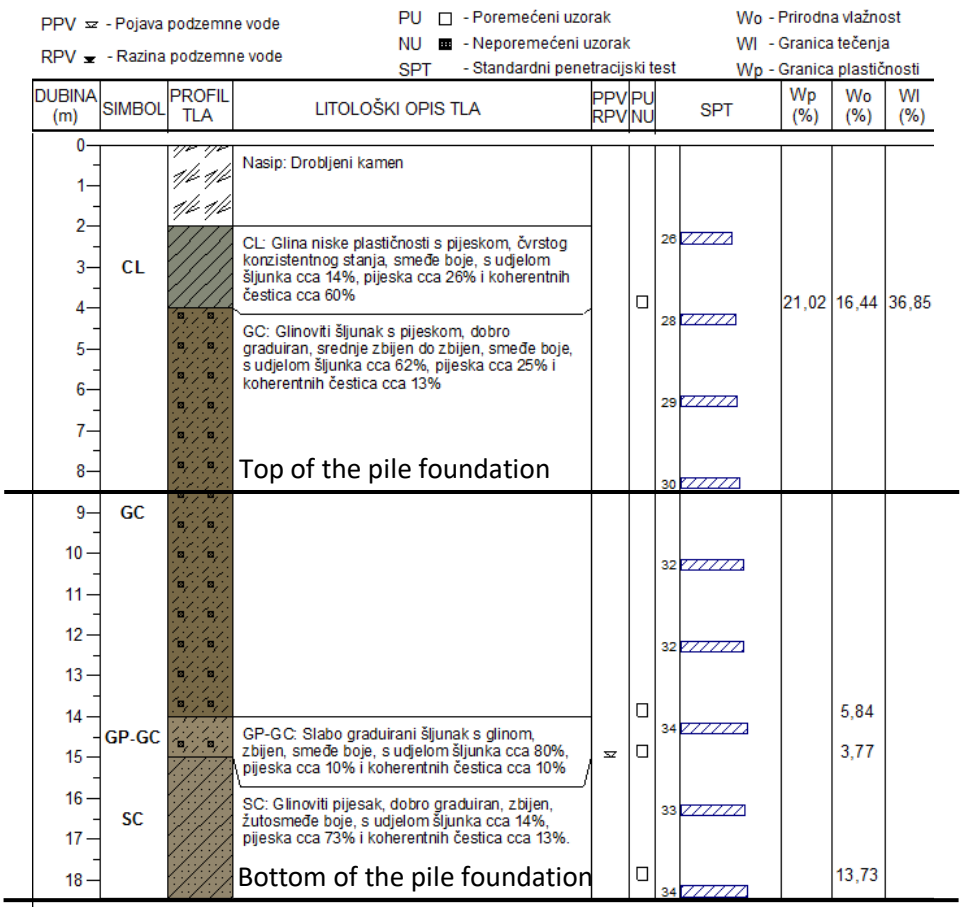

Figure 9: Borehole performed near the Karlovac Bridge embankment

3.4 Hydrological data

The hydrological data for the analysis of the two bridges was obtained from the results of deliverable D2.2 [1]. The data was obtained for the Karlovac measuring station, which is located 20 m on the upstream side of the Banija Bridge and about 400 m downstream of the Karlovac Bridge. The intensity of the flood was defined based on water height (H) and mean flow velocity (V). The hydrological situation at the measuring station is rather complex, as a stream stage-discharge curve (rating curve) shows a hysteretic behaviour (Figure 10). This indicates a non-stationary flow due to the influence of nearby effluents. The relationship between H and V is thus not uniquely defined. An estimation of the H-V relation was obtained from numerical simulations [13], which were conducted for three historical flood events from the years 2005, 2014 and 2015 (Figure 10). In this study, the results of the simulations were idealized considering three possible scenarios, i.e. a lower-bound, the best estimate and an upper-bound flow velocity scenario. All three scenarios simplistically consider a constant flow velocity for water height above the zero mark.

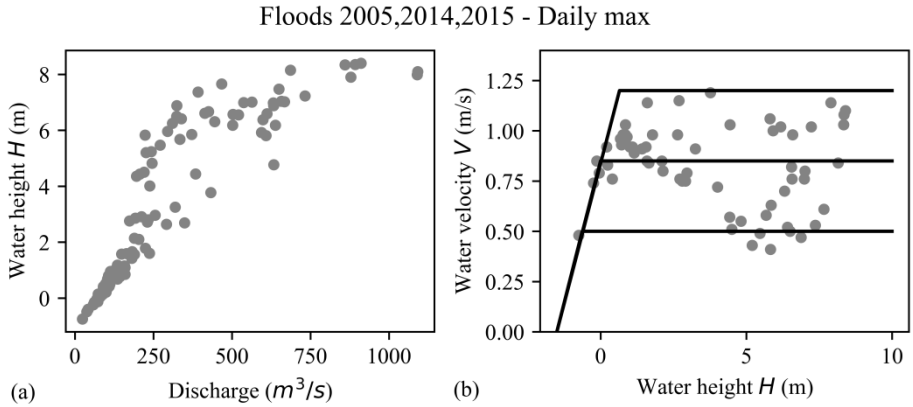

Figure 10: Daily-max relations for numerical simulation of three flood events for years 2005, 2014 and 2015 – (a) relationship between discharge and stage, (b) relationship between stage and velocity with possible idealized scenarios (lower-bound, best estimate, upper bound flow)

3.5 Measured modal properties

The measured modal parameters of both bridges were recorded on the 9th of March 2021. In the following, the most relevant results from field measurements are presented.

3.5.1 Banija Bridge

The measured modal parameters of the Banija bridge were obtained from the ambient vibration measurement campaign conducted with WP3 [5]. The results will be used for evaluation of the employed modelling approach, which will be outlined in Chapter 5. However, since only certain vibration modes of the bridge deck were excited during the measurements, the obtained results could not be used for the evaluation of the global bridge response, which is also influenced by SSI. As a result, a formal calibration of the SSI model was not possible. Nevertheless, the measurements were used to validate the vibration modes of the bridge deck. As a result of simplified modelling of the bridge deck, only translational modes of the deck were used for validation of the numerical model. Additional details regarding the modelling will be provided in Chapter 5. The translational modes of the bridge deck used for validation of the modelling approach are summarized in Table 3 and are represented in Figure 11.

Table 3: Translational modes of the bridge deck used for validation of the modelling approach for the Banija Bridge

Deck vibration mode	Frequency [Hz]	Period [s]
1st vertical	1.46	0.68
2nd vertical	2.32	0.43
1st transverse	4.76	0.21
3rd vertical	5.13	0.19

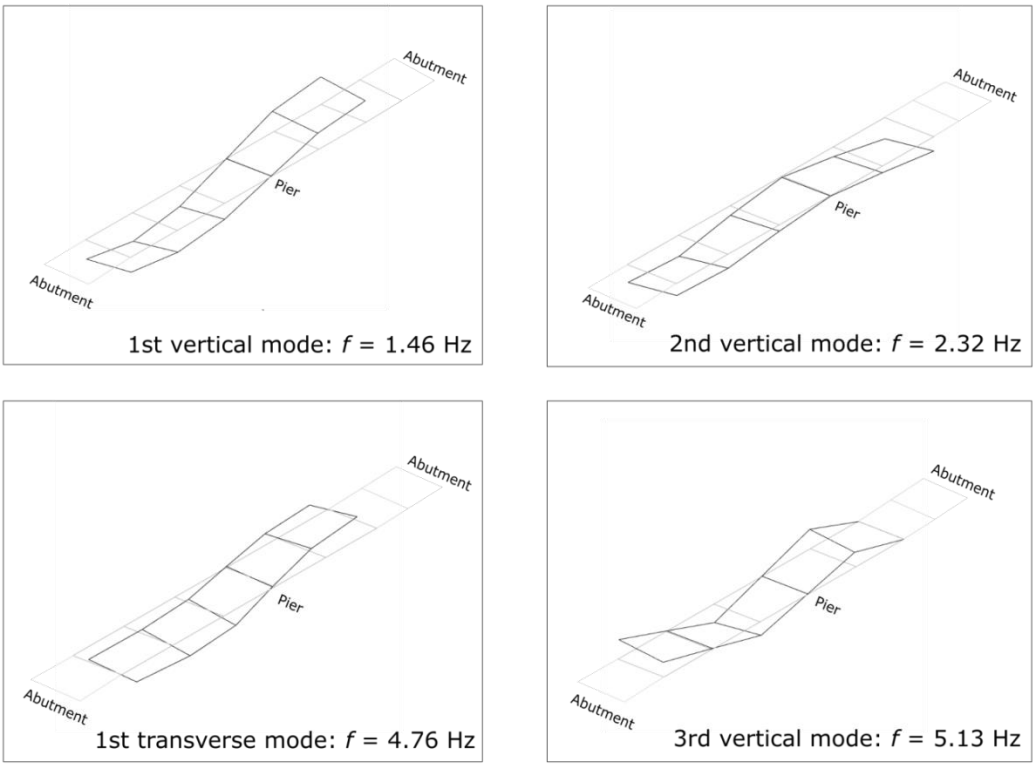

Figure 11: Translational modes of the bridge deck used for validation of the modelling approach for the Banija Bridge

3.5.2 Karlovac Bridge

The measured modal parameters of the Karlovac bridge were also obtained from the ambient vibration measurement campaign conducted within WP3 [5]. Due to difficulties in accessing the west side of the bridge with running traffic, the employed distribution of sensors focused only on the east side of the bridge. Such distribution of sensors was not optimal for the identification of the modal shape of the bridge due to difficulties in distinguishing between the vertical and torsional mode shapes. Nevertheless, it was still possible to identify four vibration modes of the bridge deck (3 translational modes and one torsional mode). The employed modes for calibration of the numerical approach are summarized in Table 4 and are represented in Figure 12. It should be noted that due to simplified modelling of the bridge deck with an equivalent beam element, only the translational modes were used for the actual validation of the modelling approach.

Table 4: Translational modes of the bridge deck used for validation of the modelling approach for the Karlovac Bridge

Deck vibration mode	Frequency [Hz]	Period [s]
1st vertical	1.65	0.61
2nd vertical	2.50	0.40
3rd vertical	4.27	0.23

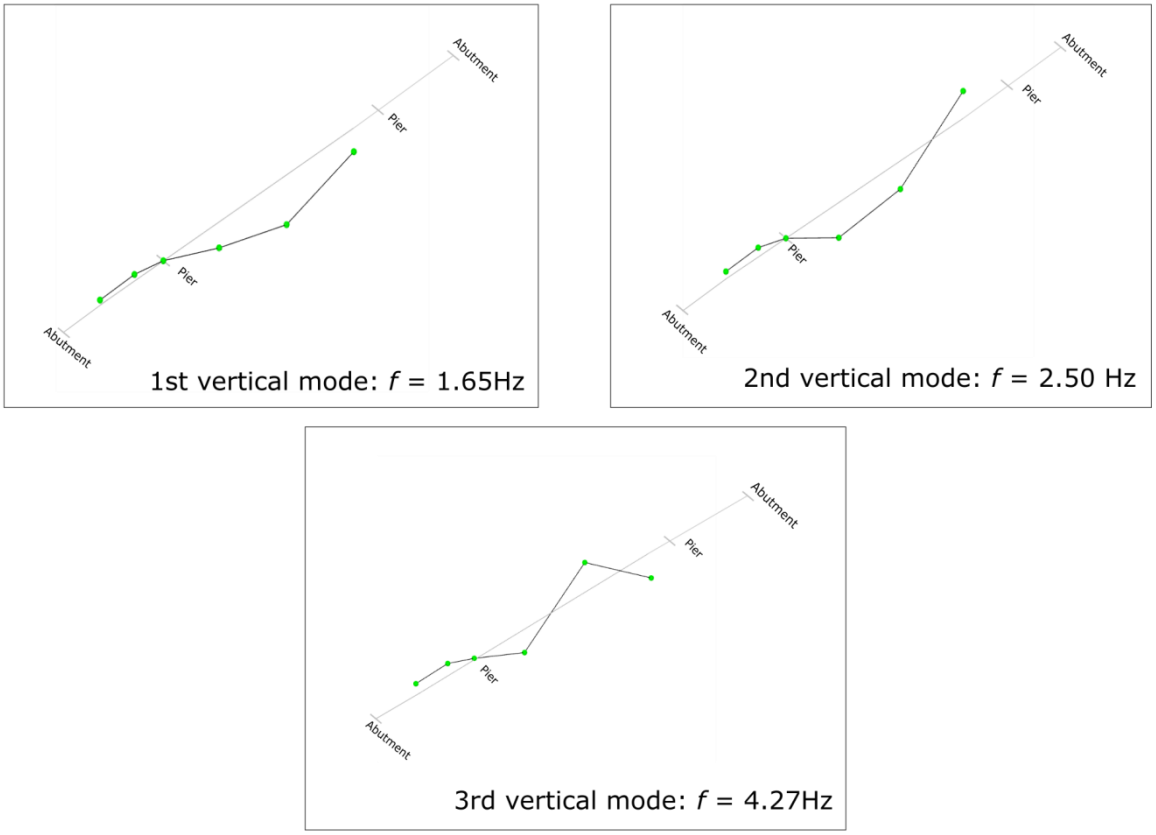

Figure 12: Translational modes of the bridge deck used for validation of the modelling approach for the Karlovac Bridge

4 Methodology for bridge vulnerability assessment

The goal of vulnerability analysis is the estimation of the probability of exceeding a designated limit state (LS) under a given level of flood intensity (Intensity Measure, IM), i.e. $P(LS|\ IM)$. The procedure used for flood fragility analysis is presented schematically in Figure 13.

Before the analysis can be performed, the flood intensity (IM) and examined limit states (LS) have to be defined. In this study, the IM was defined based on the water height (H) and mean flow velocity (V). This implies that the result of the fragility analysis is a fragility surface, which defines the probability of exceeding a designated LS for a combination of H and V (i.e. $P(LS|\ H,V)$).

Two limit states were studied: i) serviceability limit state, *SLS*, and ultimate limit state, *ULS*. The first is related to the question of whether the bridge may be in service during the flood. In contrast, the second one is related to the failure of the first component of the bridge (e.g. failure of a column, failure of bearing etc.), which is assumed to lead to failure of the bridge as a whole. Additional details regarding the definition of limit states are provided in Chapter 7.

The first step of the vulnerability analysis is the definition of a set of input flood intensity parameters, for which flood analysis is then performed. In our case, the IM was defined for the location of the Karlovac measuring station, which is located between the two bridges, 20 m upstream of the Banija Bridge and about 400 m downstream of the Karlovac Bridge (see Figure 1). A set of H values was selected, and the corresponding V values were assumed based on fixed H-V relationships. Because of the complex hydrological situation at the Karlovac measuring station (non-stationary flow), three relations H-V were used for each flood height: i) lower bound, ii) best-estimate and (iii) upper-bound. Additional details regarding the definition of the flood scenario for the two bridges were provided in Section 3.4.

For each combination of H and V, flood loads and local scour depths are first computed and used for the definition of a deterministic numerical model in accordance with the modelling approach outlined in Chapter 5. The deterministic model is then expanded with modelling uncertainties, which are introduced with consideration of random variables. Within this study, the uncertain parameters were considered to be related to the material properties of the concrete and the steel, and the geotechnical properties used for the definition of soil-structure interaction (SSI). The statistical characteristics of the considered random variables and their source references are summarized in Table 5.

Figure 13: Flowchart of the procedure for vulnerability analysis of bridges

The next step in the derivation of the flood fragility analysis is the uncertainty analysis, in which a set of N_{sim} realizations of the stochastic model are obtained by the sampling of random input

variables. As a random sampling of the variable would require a large number of simulations to be performed, variance reduction techniques such as stratified sampling are preferred for this step as they allow reduction of the required number of simulations compared to the naive Monte Carlo simulation. An efficient stratified sampling approach is offered by Latin Hypercube Sampling (LHS). In this study, the procedure for LHS sampling of the correlated variable by Vořechovský and Novák [14] was used.

An important step in the procedure is the selection of the number of simulations (N_{sim}). The required number of simulations to be performed depends on the number of random input variables (N_{var}) and the required precision of the results. Sensitivity analyses with a different number of simulations can be performed to obtain the optimal number of simulations for the examined problem. An indication of the required N_{sim} can be obtained based on the recommendation by Dolšek [15], who suggested that for practical engineering applications, it is usually sufficient that N_{sim} is about 3-times larger than the number of input variables (N_{var}). In this study, N_{sim} was set to 40, which is 5-times larger than N_{var}. The selected N_{sim} will produce a tolerance in the definition of $P(LS|\,H,V)$ of $1/40 = 0.025 = 2.5$ %, which is judged to be sufficient for practical application of the methodology.

The result of Monte Carlo simulations with LHS is a set of numerical models which are analysed to obtain an estimation of the probability of exceeding the designated LS for a given set of H and V. The $P(LS|\,H,V)$ is computed as the ratio between the number of simulations leading to exceedance of the designated LS ($N_{LS}(H,V)$) and the total number of simulations N_{sim} as follows:

$$P(LS|\,H,V) = \frac{N_{LS}(H,V)}{N_{sim}}. \quad (1)$$

Table 5: Considered random variables for flood fragility analysis of the case study bridges.

Parameter:	Distribution:	Reference:
Concrete strength	Normal ($\mu = 1, COV = 0.20$)	[16]
Steel yield strength	Lognormal ($\tilde{m} = 1,\ COV = 0.07$)	[17]
Steel elastic modulus	Lognormal ($\tilde{m} = 1,\ COV = 0.03$)	[17]
Soil shear modulus	Lognormal ($\tilde{m} = 1,\ COV = 0.30$)	[18], [19]
Soil friction angle	Normal ($\mu = 1, COV = 0.12$)	[18], [19]
Soil saturated weight	Normal ($\mu = 1, COV = 0.10$)	[19]
Soil N_{60}	Normal ($\mu = 1, COV = 0.15$)	[20]
Hydrodynamic pressure	Normal ($\mu = 1, COV = 0.10$)	[21]
Scour depth	Lognormal ($\tilde{m} = 0.68,\ COV = 0.16$)	[22]

5 Numerical modelling approach

In this section, the numerical modelling approach for the two case study bridges is described. The structural modelling of both bridges was done with a similar approach, whereas the modelling of SSI was slightly different due to different foundation types, i.e. squat well foundations vs pile foundations. Both numerical models were constructed in the OpenSeesPy Library [23], which is an open-source Python3 interpreter for OpenSees [24]. As OpenSees does not provide a user-friendly graphical interface, an initial numerical model of two bridges was developed in CSI SAP2000 [25]. The models were then imported in OpenSeesPy and extended with the modelling of soil-structure-interaction (SSI) via a set of user-defined Python scripts. The numerical models of the case study bridges are depicted in Figure 14 and Figure 15.

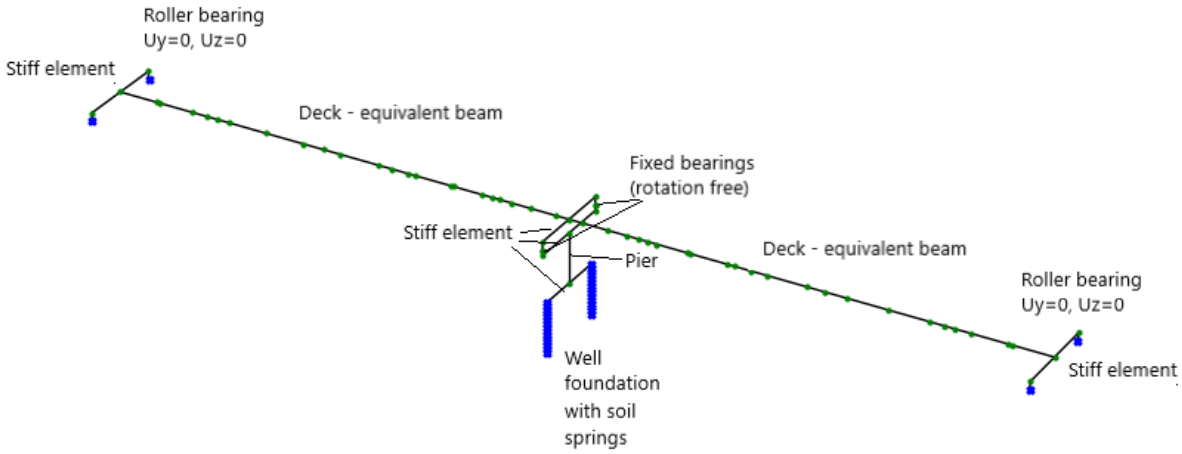

Figure 14: Numerical model of the Banija Bridge

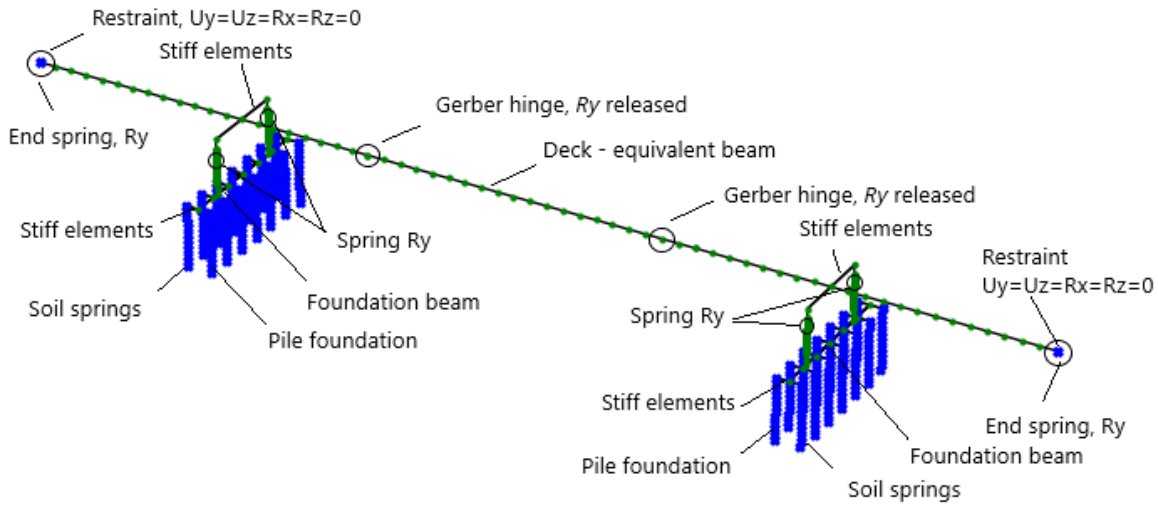

Figure 15: Numerical model of the Karlovac Bridge

5.1 Structural modelling

In both models, the bridge superstructure and foundations were modelled with linear elastic Timoshenko beam-column elements. The geometry, section properties and material characteristics were imported from the previously defined CSI SAP2000 model [25].

5.1.1 Banija Bridge

The deck of the bridge was modelled with an equivalent beam element. The stiffness of the equivalent beam was calibrated based on the results of a more precise beam-shell model constructed in CSI SAP2000 [25]. The variable stiffness of the deck due to changing thicknesses of the main girder flanges was considered by subdivision of the beam element in several elements. The pier and the two well foundations were also subdivided along with their height in elements of length 0.1 m. The correct offset between centroids of different elements was achieved by the use of rigid elements. These were used to support the deck at the location of the bearings and to connect the pier to the well foundations. The rigid elements were considered to be infinitely stiff and massless. The boundary conditions at the abutments were such to simulate the behaviour of the roller bearings, i.e. free translation in the longitudinal direction and free rotations. The bearings at the pier were modelled as fixed against translation and free for rotation.

5.1.2 Karlovac Bridge

The deck of the Karlovac Bridge was also modelled with an equivalent beam element. Three sections were assigned to the equivalent beam in order to account for different height and section characteristics of the deck. The stiffness of the equivalent beam was calibrated based on the results of a more precise beam-shell model constructed in CSI SAP2000 [25]. The deck was considered to rotate freely at the location of the Gerber bearings, while the translations were restrained. The connection between the deck and the two piers was achieved by the employment of rigid elements. At the top of the columns, the deck was assumed to be partly restrained against rotation due to the non-ideal construction of the elastomer bearing. Results of the bridge inspection [8] indicated that the joints are filled with excess concrete from the construction of the deck. The stiffness of the rotational spring at the top of the columns was calibrated based on the results of ambient vibration measurements. The calibration process indicates that 20%-partial fixity was appropriate to reproduce the measured modal frequencies. The base of the piers was connected to the piles with rigid elements. The piers and the pile foundations were subdivided along with their height in elements of length 0.1 m. In the case of the pier, the subdivision allowed for a more precise definition of flood loading, while in the case of piles, the subdivision was employed for the application of soil springs, used for simulation of SSI. The boundary conditions at the abutments were such to simulate free translation in the longitudinal direction and partial restrain against the rotation of the deck. All other degrees of freedom were assumed to be fixed. Following a calibration process, a 20%-partial fixity against rotation was found to lead to good agreement with measured modal frequencies.

5.2 Soil-structure interaction

In both numerical models, the SSI was considered with a set of distributed non-linear springs, which connect the foundation nodes to fixed restrains. The definition of the soil springs in the two models differs due to the different foundation types of the two bridges. The Banija Bridge is founded on two large-diameter well foundations, which behave differently than the pile foundation of the Karlovac Bridge, for which the traditional *p-y*, *t-z*, *q-z* spring approach is applicable. As a result, a modified approach was used for the SSI modelling of the Banija Bridge.

5.2.1 Banija Bridge

As a result of the well foundations having a small ratio between the length and diameter ($L/D = 0.90$), the traditional *p-y*, *t-z*, *q-z* spring approach developed for slender piles was extended with the addition of a moment rotation (M_b-φ_b) and a translation spring (H_b-u_b) at the base of the foundation in accordance with the approach suggested by Van Impe and Wang [26]. A modification of the subgrade reaction of the *p-y* springs was necessary to account for the fact that the traditional approach does not consider the contribution of the shaft friction, which increased the stiffness of soil subgrade reaction.

The force-displacement relationship of the *p-y*, *t-z* and *q-z* springs was modelled with OpenSees materials PySimple1 [27], TzSimple1 [28], and QzSimple1 [29]. The input parameters for the definition of the materials are the ultimate forces (P_u, T_u, Q_u) and displacements at 50% ultimate force (y_{50}, z_{tz50}, z_{qz50}). Additional *SoilType* parameters define the shape of the backbone curve based on available implementations from literature. The moment-rotation and force-displacement relationship of the M_b-φ_b and H_b-u_b springs was modelled with the elastic-perfectly-plastic OpenSees material *ElasticPP* [30], which is defined by initial tangent stiffness and rotation (displacement) when the material reaches the plastic state (tangent goes to zero).

In the case of the *p-y* springs, the backbone curve was calculated according to API 2003 [31] recommendations for cohesionless soils (*SoilType* = 2). The ultimate force of springs was computed according to Reese and Van Impe's [32] equation:

$$P_u = \overline{A_s}\, p_u\, \Delta z \tag{2}$$

where $\overline{A_s}$ is the normalized resistance factor that depends on the ratio z/D, z is the depth of the spring, D is the diameter of the well, p_u is the ultimate soil resistance per unit length computed from Eq. 3.44 and 3.55 in [32], and Δz is the vertical spacing of the springs. The displacement at 50% capacity (y_{50}) was calculated based on the API 2003 [31] hyperbolic load-displacement curve:

$$y_{50} = \frac{\overline{A_s}\, p_u}{k\, z} \operatorname{atanh}(0.5) \tag{3}$$

where k is the subgrade reaction, which depends on the soil density (friction angle) and varies for saturated and unsaturated conditions. As a result of a preliminary study indicating that the obtained stiffness of the foundation was too small compared to the elastic stiffness of embedded

shallow foundations (e.g. [33]), the subgrade reaction k from API 2003 [31] had to be multiplied with a factor of 5 to match the modal characteristics which will be obtained for lumped-springs SSI model of shallow foundations. The correction of the stiffness was necessary because the traditional *p-y* approach was developed for small diameter slender piles, for which the contribution of shaft friction is insignificant and is typically disregarded. In the case of a large-diameter pile foundation, the effect of shaft friction becomes important and can be approximately considered with an increase of subgrade reaction of the soil, as suggested by Van Impe and Wang [26].

The backbone curve for *t-z* springs was defined according to Mosher's [34] recommendations (*SoilType* = 2). The ultimate force of the spring was computed based on Mohr-Coulomb failure criteria:

$$T_u = K\,\sigma_v'\,\tan(\delta)\,\pi\,D\,L_{tr} \tag{4}$$

where the coefficient of lateral pressure is taken as K=1.0 (full displacement piles), σ_v' is the effective vertical stress and δ is the friction coefficient of the soil-foundation interface, considered equal to 0.9 φ. The displacement at 50% capacity (z_{tz50}) was assumed to amount to 0.05 inch (1.27 mm) according to API 2005 [35] bi-linear force-displacement relationship for sands.

The backbone curve of the *q-z* springs was defined according to Vijayvergiya's [36] recommendations (*SoilType* = 2). The ultimate bearing force at the tip of the well was computed according to the Meyerhof method [37] for shallow foundations ($D_f < D$):

$$Q_u = \left[c\,N_c\,d_c + \gamma\,D_f\,N_q\,d_q + 0.5\,\gamma\,D\,N_\gamma\,d_\gamma\right]\pi\frac{D^2}{4} \tag{5}$$

where N_c, N_q , N_γ and d_c, d_q, d_γ are the bearing and depth correction factors according to [37], respectively, and D_f is the depth of the foundation. The displacement (settlement) at 50% capacity was computed according to the Burland and Burbidge SPT method [38]:

$$z_{qz50} = q_{net,50}\,\frac{1.71}{\overline{N}_{60}^{1.4}}\,B^{0.7} \tag{6}$$

where $q_{net,50}$ is the net overburden pressure at 50% capacity (gravity loads are subtracted to considered previous consolidation), $\overline{N}_{60}$ is the average value of N_{60} blows in the influence zone of the foundation, and B is the foundation width.

The initial rotational stiffness $(K_{\varphi b})$ of the M_b-φ_b spring at the base of the foundation was computed based on the solution for the shallow foundation on elastic soil (e.g. [33]). The rotation at the full mobilisation of the M_b-φ_b spring was computed as:

$$\theta_{pb} = \frac{M_{ub}}{K_{\varphi b}} = \frac{3\,M_{ub}\,(1-\nu)}{8\,(G\,R^3)} \tag{7}$$

where M_{ub} is the foundation's ultimate moment capacity at the base, G and ν are the shear modulus and Poisson's ratio of the soil, and R is the radius of the foundation. The M_{ub} was

computed based on the Meyerhof method [37] using an iterative procedure in which the applied moment was increased progressively until the soil reaction at the base could no longer support the applied load.

The initial stiffness of H_b-u_b spring (K_{hb}) at the base of the foundation was computed by dividing the ultimate sliding resistance (H_{ub}) by the displacement at the full mobilisation of the resistance (u_{pb}). Considering the definition of H_{ub} according to API 2005 [35], the initial stiffness K_{hb} is computed as:

$$K_{hb} = \frac{H_{ub}}{u_{pb}} = \frac{c'A + Q \tan \varphi'}{u_{pb}} \quad (8)$$

where c' and φ' are the effective cohesion and shear angle of the soil, A is the area of the foundation base, and Q is the applied vertical load on the foundation base. According to the recommendation by Van Impe and Wang [26], the sliding resistance can be considered to fully mobilise at a displacement of 5 mm (u_{pb} = 5 mm).

5.2.2 Karlovac Bridge

The soil-structure interaction for pile foundations of the Karlovac Bridge was modelled with the traditional *p-y, t-z, q-z* spring approach. In this approach, the *p-y* springs simulate the horizontal resistance of the soil, while the *t-z* springs simulate the friction over the shaft. An additional *q-z* spring is located at the base of the pile and is used to simulate the bearing capacity of the pile tip. The force-displacement relationship of the *p-y*, *t-z* and *q-z* springs was modelled with OpenSees materials PySimple1 [27], TzSimple1 [28], and QzSimple1 [29]. The input parameters for the definition of the materials are the ultimate forces (P_u, T_u, Q_u) and displacements at 50% ultimate force (y_{50}, z_{tz50}, z_{qz50}). Additional *SoilType* parameters define the shape of the backbone curve based on available implementations from literature.

The backbone curve of the *p-y* spring was calculated according to API 2003 [31] recommendations for cohesionless soils (*SoilType* = 2). The ultimate force (P_u) and displacement at 50% ultimate force (y_{50}) were computed using Eq. (1) and (2) from Section 5.2.1, considering the subgrade reaction k by API 2003 [31].

The backbone curve for *t-z* springs was defined according to Mosher's [34] recommendations (*SoilType* = 2). The ultimate force (Q_u) and displacement at 50% ultimate force (z_{tz50}) were computed in the same way as in the case of the Banija Bridge (see Section 5.2.1).

The backbone curve of the *q-z* springs was defined according to Vijayvergiya's [36] recommendations (*SoilType* = 2). The ultimate bearing force at the tip of the pile was computed according to the Meyerhof method for pile foundation [39]:

$$Q_u = \left[c' N_c^* + \mathrm{q}' N_q^*\right] \pi \frac{D^2}{4} \quad (9)$$

where c' is the effective cohesion (considered 0 in this study), q′ is the effective vertical stress at the tip of the foundation, and D is the diameter of the pile. N_c^* and N_q^* are the bearing capacity

factor for pile foundations according to [39]. The displacement (settlement) at 50% capacity (z_{qz50}) was computed based on the Vijayvergiya's [36] force-displacement relation:

$$z_{qz50} = 0.125\, z_c \tag{10}$$

where z_c is the displacement at the mobilization of full bearing capacity, which was assumed to be attained at a displacement of 5% of the pile diameter.

5.3 Load modelling

The loads considered on the structure in the study were gravity loads, hydrodynamic loads, buoyancy and debris loads. The loads were combined to produce the maximum possible overturning action on the bridge, which happens when horizontal hydrodynamic and debris loads are combined with an uplift action on deck. In such a case, the hydrodynamic uplift of the deck was combined with buoyancy. For this reason, the concurrent presence of traffic loads was not considered as it would result in a stabilising action on the bridge. The hydrodynamic loads were only applied on the areas not affected by debris (no concurrent action with debris).

The calculation of individual loads is described in the following sections. The loads were calculated per unit length of individual components and were applied in the model as uniformly distributed loads.

5.3.1 Gravity loads

The gravity load on the structure is considered the self-weight of elements and permanent loads of finishes on the bridge deck. The loads were computed based on the geometry of the elements (e.g. section area) and the specific weight of the material.

5.3.2 Hydrodynamic loads

The hydrodynamic forces were computed according to Australian code AS5100.2-2004 [40]. The drag force in the direction of the flow is defined with the equation:

$$F_d = 0.5\, C_d\, V^2\, A_d \tag{11}$$

where C_d is the drag coefficient, V is the average water velocity and A_d is projected wetted area in the direction of the flow. For piers with semi-circular nosing, the coefficient C_d equals to 0.7, while for square-end columns C_d equals to 1.4. In the case of bridge decks, the coefficient C_d is computed as a function of relative submergence of the deck (S_r) and proximity ratio (P_r), which are defined as:

$$S_r = \frac{d_{wgs}}{d_{sp}} \quad \text{and} \quad P_r = \frac{y_{gs}}{d_{ss}} \tag{12}$$

where d_{wgs} is the distance from the girder soffit to flood water surface, d_{sp} is the wetted depth of deck (including any railing and parapets), y_{gs} is the average vertical distance from the girder soffit to the riverbed, and d_{ss} is the wetted depth of the solid superstructure (excluding railing but including parapets).

The uplift force on the bridge deck is computed with the following equation:

$$F_l = 0.5\, C_l\, V^2\, A_l \tag{13}$$

where C_l is the lift coefficient, and A_l is the wetted area in the direction perpendicular to the flow. The lift force on a submerged deck is acting in the vertical direction. The coefficient C_l depends on the relative submergence of the deck (S_r). Two possible combinations of the lift forces are prescribed: i) an upward lift force for the verification of overturning and calculation of tie-down forces, and ii) a downward force verification of the deck and foundations. For the purpose of this study, the lift force on the deck was assumed to act in the upward direction and was combined with buoyancy forces, as will be described in the next section.

Triangular distribution of hydrodynamic forces was assumed in accordance with [41] as results of a preliminary study indicated to produce larger actions on the bridge compared to the uniform distribution. The loads were applied as uniformly distributed loads on the elements with a value of $2F_d$ ($2F_l$) at the top of water flow and value zero at the bottom.

5.3.3 Buoyancy

The standard AS5100.2-2004 [40] defines that in the case of the verification of overturning and calculation of deck tie-down forces, a vertical uplift force buoyancy force has to be considered to act on the partly or fully submerged bridge deck. The buoyancy force is computed as the weight of the displaced fluid and is applied concurrently with the upward lift force on the bridge deck. The buoyancy force increase with the submergence of the deck and reaches its maximum value when the deck is fully submerged. In this study, the buoyancy force was combined with hydrodynamic uplift forces.

5.3.4 Debris forces

Severe flooding can result in the accumulation of debris on the bridge piers and superstructure. The debris forces were calculated according to Australian code AS5100.2-2004 [40]. The depth of the debris mat varies depending on factors such as catchment vegetation, available water flow depth and superstructure span. The standard AS5100.2-2004 specifies the height of the debris (H_d) mat to be between 1.2 m and 3 m. In this study, H_d was assumed to amount to 2.1 m.

In the case of bridge piers, the width of the debris mat (W_d) is assumed to be equal to one half of the sum of the adjacent spans or 20 m, whichever is smaller. The top of the debris mat is assumed to be located at the top of the flood level. In the case of the bridge deck, the projected length of the debris mat is equal to the projected length of the deck. The loads are applied at the mid-height of the deck, including any railing or parapets. The debris forces are calculated with Equation (11) considering separate drag coefficients (C_d) for bridge piers and decks. Both factors depend on

flood height (H) and mean flow velocity (V). The factor C_d for debris on the deck additionally depends on the proximity ratio (P_r).

5.4 Scour modelling

5.4.1 Local scour

For each flood scenario, the depth of local pier scour was computed according to the HEC-18 [42] equation:

$$y_s = \left[2.0\ K_1\ K_2\ K_3\ \left(\frac{H}{a}\right)^{0.35}\ Fr^{0.43}\right]\ a \tag{14}$$

where K_1, K_2, K_3 are correction factors for pier nose shape, angle of attack of flow (θ), riverbed conditions, respectively, and a is the pier width. Fr is the Froude number defined as:

$$Fr = \frac{V}{(g\ H)^{1/2}} \tag{15}$$

Where V is the mean flow velocity upstream of the pier, g is the acceleration of gravity, and H is the flow depth upstream of the pier. For round-nose piers and angle of attack of flow $\theta = 0$, the coefficients K_1 and K_2 amount to 1.0. For clear-water scour, K_3 equals to 1.1. For square-nose piers, the coefficient K_1 amount to 1.1. The sketch of the HEC-18 pier scour model is presented in Figure 16 (note that the parameter H corresponds to y_1 in the Figure 16).

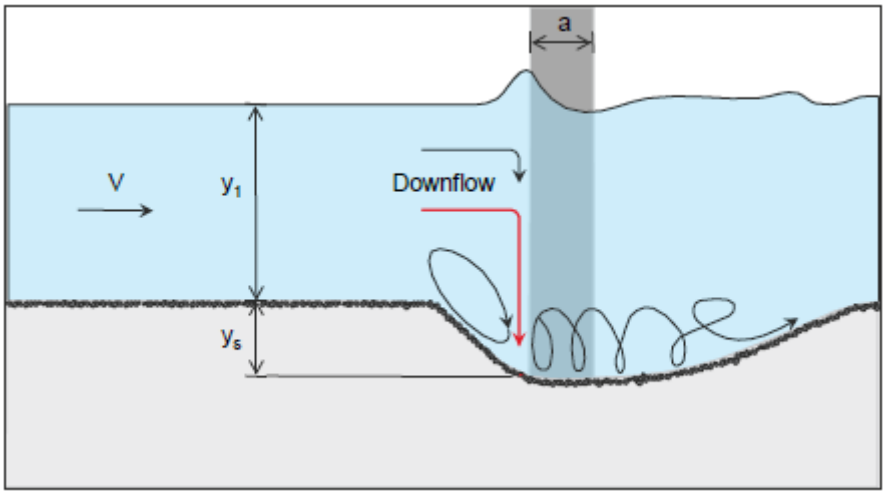

Figure 16: Sketch of the HEC-18 pier scour model [42]

5.4.2 Effect of scour on soil-structure interaction

The effect of local scour was modelled by not assigning SSI springs, defined in Section 5.2, in the part of the foundation affected by scour. This results in a decrease of the horizontal stiffness and increase of vertical settlement of the bridge due to a smaller embedded length of the foundation.

5.4.3 Effect of scour on loading

In addition to the effect on the stiffness of the foundation, scour can lead to exposure of the foundation to additional hydrodynamic flow loads, as the foundation is no longer shielded by soil. This effect was considered by assigning additional drag forces on the scouring part of the foundation.

5.4.4 Influence of debris on local scour

Debris accumulation against the pier can result in an increase in scour depth due to constriction and redirection of the water flow. The effect of debris on the local scour of the pier was considered according to the recommended approach proposed by Lagasse et al. [43]. The approach relies on the quantification of the equivalent pier width (a_d^*), which is then used in Equation (12) for quantification of the scour depth with consideration of debris. The equivalent pier width is defined as:

$$a_d^* = \frac{K_{d1}(H_d\, W_d)\,(L_d/H)^{K_{d2}} + (H - K_{d1}\, H_d)\, a}{H} \quad \text{for} \quad L_d/H > 1.0$$

$$a_d^* = \frac{K_{d1}(H_d\, W_d) + (H - K_{d1}\, H_d)\, a}{H} \quad \text{for} \quad L_d/H \leq 1.0 \tag{16}$$

where K_{d1} and K_{d2} are experimentally obtained factors, which depend on the shape of the debris raft ($K_{d1} = 0.79$ and $K_{d2} = -0.79$ for rectangular debris raft; $K_{d1} = 0.21$ and $K_{d2} = -0.17$ for triangular debris raft), W_d is the width of the debris raft normal to the flow, H_d is the height of debris raft, L_d is the length of the debris upstream from the pier face, and H is the depth of the approaching flow. In the study, the length of the debris was assumed to be equal to the water height ($L_d/H = 1.0$), which produces the largest amplification of scour for a given water height.

6 Validation of the numerical approach

The numerical approach from Chapter 5 was validated against measured modal properties. Since only vibration modes of the bridge deck were excited during the measurements, the obtained results could not be used for the evaluation of the global bridge response. Nevertheless, the measurements were used to validate the vibration modes of the bridge deck.

6.1 Banija Bridge

The comparison of the calculated and measured modal periods of the Banija Bridge is presented in Table 6. The global vibration modes that could be detected during the measurement (due to lack of excitations) are marked as "ND" – "Not detected".

As it can be seen from the table, the calculated translational periods of the bridge deck match very closely with the measured values. A good agreement was also obtained for the modal shapes presented in Figure 17. A phase shift of 180 degrees can be observed for the modes with the exception of the first vertical mode, but they are actually representing the same vibration mode.

Based on the results, it can be concluded that the employed modelling approach leads to a reliable prediction of the bridge stiffness and mass.

Table 6: Comparison of the calculated and measured modal periods of the Banija Bridge

Description	Period (s) - Calculated	Period (s) - Measured
1st vertical mode of the deck	0.67	0.68
Global longitudinal mode	0.60	ND
2nd vertical mode of the deck	0.42	0.43
Global transverse mode	0.36	ND
Global vertical mode	0.24	ND
1st transverse mode of the deck	0.21	0.21
3rd vertical mode of the deck	0.18	0.19

ND … not detected

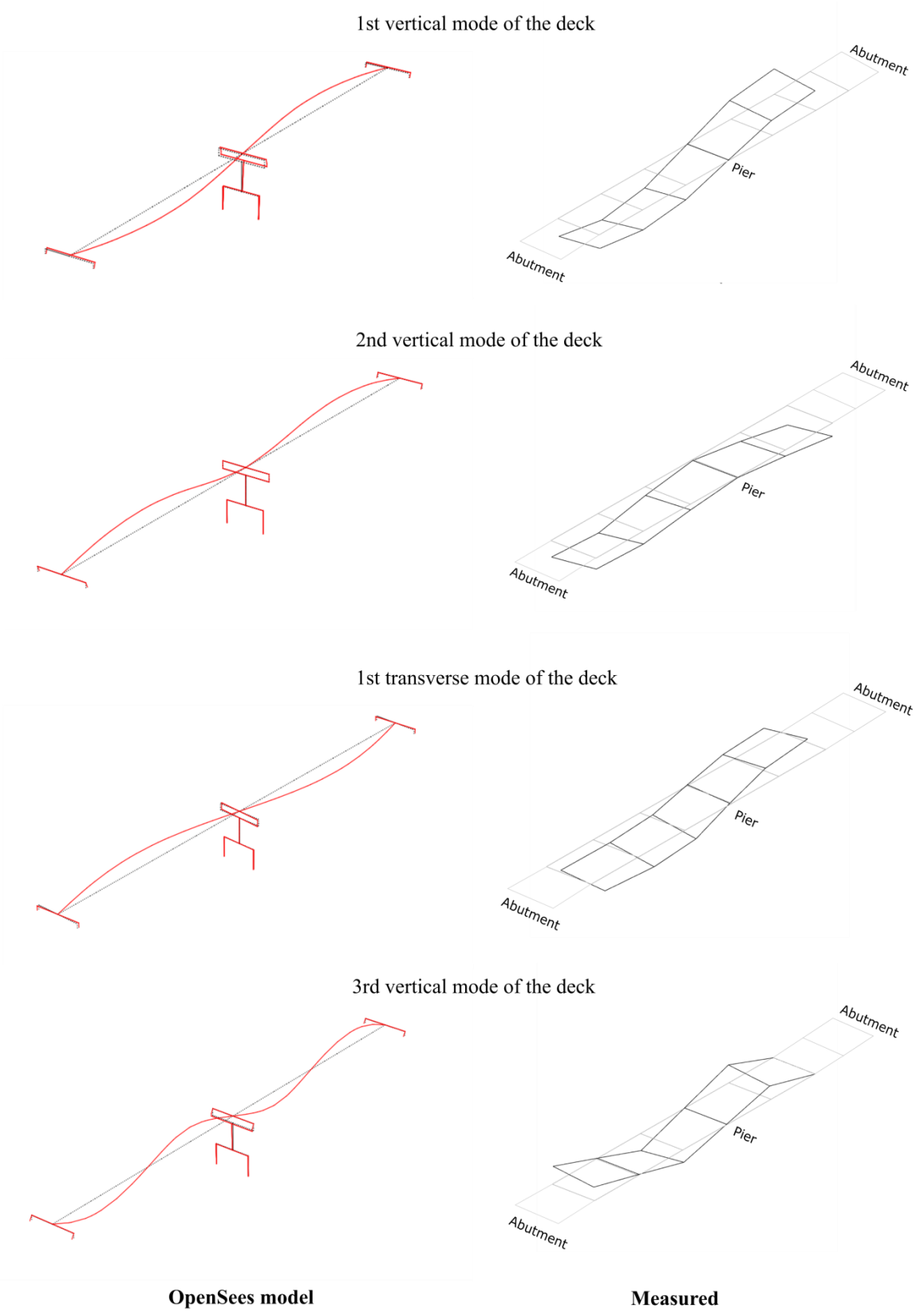

Figure 17: Comparison of the calculated and measured vibration modes of the Banija Bridge

6.2 Karlovac Bridge

The comparison of the calculated and measured modal periods of the Karlovac Bridge is presented in Table 7. Due to limited information regarding the shape of the vibration modes (limitation of employed distribution of sensors due to on-going high volume traffic), the calculated vibration periods are presented for two numerical models: i) CSI SAP 23 beam-shell model (no SSI), ii) OpenSees beam model with consideration of SSI, later used in Section 7. This is done to provide a better representation of the vibration modes. It should be noted, however, that the CSI SAP 23 model does not consider SSI. This means that the model itself is less reliable than the OpenSees model.

Table 7: Comparison of the calculated and measured modal periods of the Karlovac Bridge

Description	Period (s) – Calculated CSI SAP 23 model	Period (s) – Calculated OpenSees model	Period (s) - Measured
Global longitudinal mode	/ *	0.69	ND
1st vertical mode of the deck	0.60	0.61	0.61
2nd vertical mode of the deck	0.42	0.35	0.40
Global transverse mode	0.15	0.22	ND
3rd vertical mode of the deck	0.22	0.22	0.23

* Mode present in combination with second bending mode
ND … Not detected

As it can be seen from Table 7, the calculated modal periods from the OpenSees model match very well with the measured periods from ambient vibration measurements. It should be noted that this conclusion only applies to bending modes of the bridge deck. Unfortunately, the global horizontal modes of the bridge could not be validated due to the lack of excitation in the horizontal modes during ambient vibration measurements.

A good agreement was also obtained for the modal shapes presented in Figure 18. A phase shift of 180 degrees can be observed in all the modes, but the overall shape matches very well.

It can be concluded that the employed modelling approach leads to a reliable prediction of the bridge stiffness and mass.

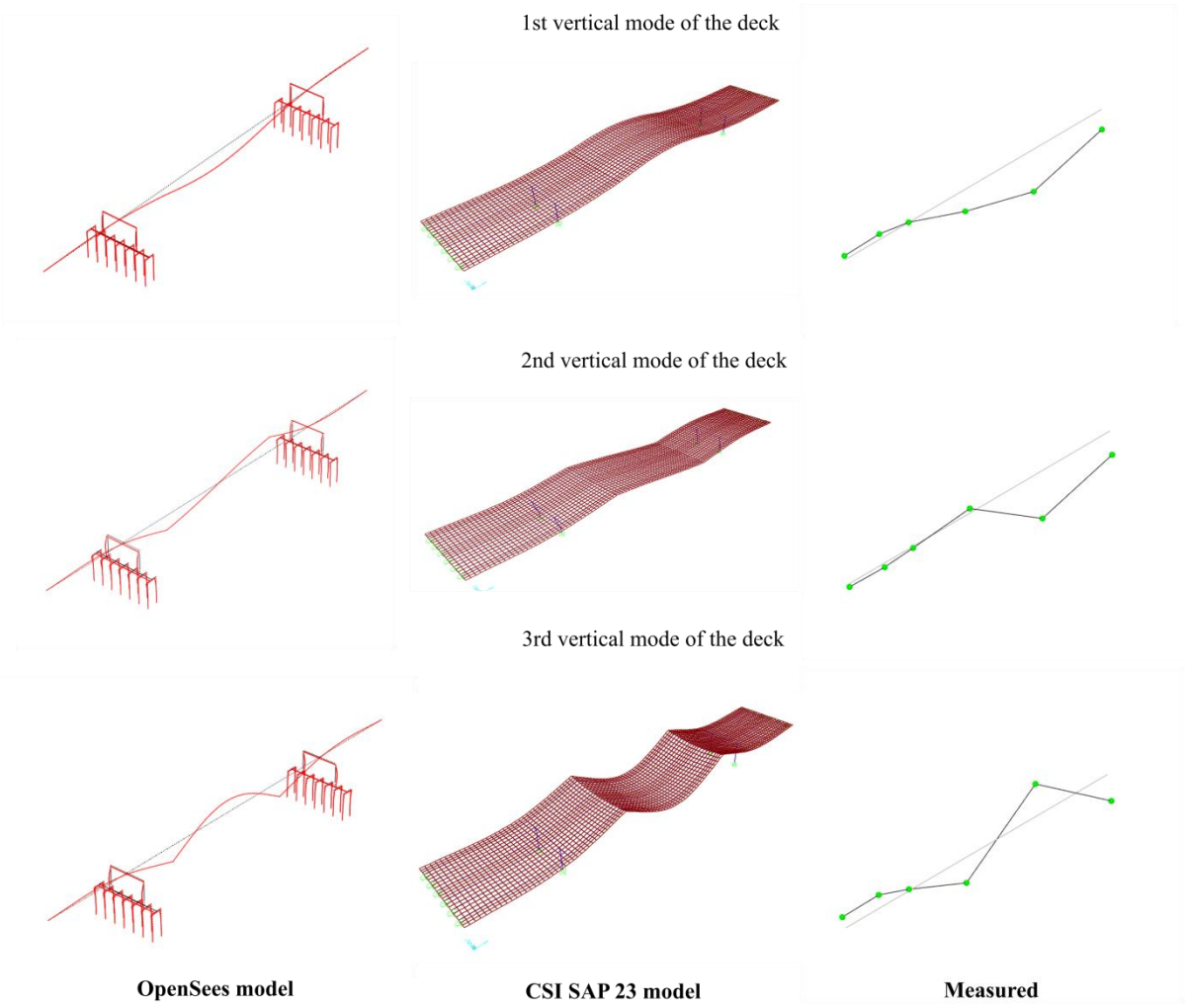

Figure 18: Comparison of the calculated and measured modal vibration model of the Karlovac Bridge

7 Vulnerability analysis and results

This section presents details regarding the vulnerability analysis of the two case study bridges and their results. Two limit states (LSs) and three flooding scenarios were considered. The considered LSs are the serviceability and the ultimate limit state of the bridge (SLS and ULS). The SLS was defined based on the exceedance of a threshold value of scour and water height, whereas the ULS was defined based on the failure of the first component of the bridge. The definition of LSs is provided separately for the Banija Bridge and the Karlovac Bridge in sections 7.1 and 7.2, respectively.

Different flood loading scenarios were considered for the SLS and ULS. The considered flood loading scenarios for the SLS considered the potential for debris accumulation of different sizes. The flood loading scenarios for the SLS are thus the following:

- No debris accumulation on the pier (*No debris*)
- Small-size accumulation of debris on the pier with dimensions W_d / H_d = 5 m / 2.1 m, which in the perpendicular direction of the flow cover about 5% of the total bridge span or equivalently about 2-times the height of the deck (*Small debris*)
- Medium-size accumulation of debris on the pier with dimensions W_d / H_d = 10 m / 2.1 m, which in the perpendicular direction of the flow cover about 10% of the total bridge span or equivalently about 4-times the height of the deck (*Medium debris*)
- A large accumulation of debris on the pier with dimensions W_d / H_d = 20 m / 2.1 m, which in the perpendicular direction of the flow cover about 20% of the total bridge span or equivalently about 8-times the height of the deck (*Large debris*).

It should be noted that debris accumulation on the deck is not considered because a flood height exceeding the height of the pier (7.5 m) is considered to trigger the exceedance of the SLS already.

In the case of ULS, a different level of detail of the analysis was performed for the two case study bridges. For the Banija Bridge, a fully probabilistic fragility analysis was performed, while for the Karlovac Bridge, only a deterministic flood analysis was undertaken due to two reasons: i) failure of the bridge is not expected (results of the preliminary analysis indicated low utilization ratios of the bridge), ii) lack of data regarding the structural materials and disposition of reinforcement, which limit the precision of such analysis significantly.

Debris is also considered in the examination of the ULS of the two bridges. In this case, only large debris with dimensions W_d / H_d = 20 m / 2.1 m is considered because smaller debris is not expected to trigger the failure of the bridges. The considered flood loading scenarios for the ultimate LS are the following:

- No debris accumulation (No debris)
- Debris accumulation and scour, but no amplification of scour due to debris (Debris, with no amplification of scour)
- Debris accumulation and amplification of scour due to debris (Debris, with amplification of scour).

The results of the fragility analysis are presented in sections 7.1 and 7.2, separately for the Banija Bridge and the Karlovac Bridge.

7.1 Banija Bridge

7.1.1 Definition of limit states

In the case of the Banija Bridge, the SLS was defined based on the exceedance of the scour depth of 50% of the foundation height (2.8 m) and water height reaching the top of the pier (water height still 0.70 m below the bridge deck). The selected threshold values are assumed to be the limit value that no longer provides safe operation of the bridge.

The ULS was defined with the failure of the first component. The following failure mechanisms were considered:

- Bending and shear failure at the base of the pier
- Shear failure of the steel bearings above the pier and the abutments
- Bending failure of the deck at the middle of the first span
- Bearing failure of the foundation (vertical & bending capacity at the base)

The calculation of the failure mechanism is based on the capacity of the members, where no safety factors were considered. The bending capacity of the pier was conservatively defined based on the section modulus of the pier and the mean tensile strength of concrete C25/30 according to EN-1992-1-1 [7]. The contribution of reinforcement was not considered because it was assumed that amount of reinforcement is below minimum code requirements [7]. The shear strength of the pier was calculated according to equation (6.2.a) from [7], which is applicable for a member without shear reinforcement. Shear capacities of the shear pin at the middle bearing and the shear keys at the abutment bearing were computed considering the elastic shear resistance according to EN-1993-1-1 [6], assuming a yield strength of the steel of 235 MPa. The bending capacity of the deck was defined based on the section modulus of the deck in the transverse direction and yield strength of the steel of 235 MPa. The failure of the foundation was verified by comparing the applied load to the vertical and bending capacity of the foundation base computed according to the Meyerhof method [31].

7.1.2 Results for serviceability limit state

The results of the analysis were the following fragility surfaces for the serviceability limit state:

- Flood fragility surface for serviceability limit state (No debris scenario) (Figure 19)
- Flood fragility surface for serviceability limit state (Small debris scenario) (Figure 20)
- Flood fragility surface for serviceability limit state (Medium debris scenario) (Figure 21)
- Flood fragility surface for serviceability limit state (Large debris scenario) (Figure 22).

The fragility surfaces represent the probability of exceedance of the serviceability limit state for a given combination of water height and velocity. The values of the fragility curves are thus between 0 and 1. A summary of the probabilities of exceeding the SLS for different flood scenarios and sizes of debris is presented in Table 8. A colour code is used in the table to ease understanding of the likelihood of exceeding the serviceability limit state: i.e. green colour for low likelihood ($P(SLS|H,V) < 0.33$), orange color for medium likelihood ($0.33 \leq P(SLS|H,V) < 0.66$), and red colour for high likelihood ($P(SLS|H,V) \geq 0.66$).

As it can be seen from Figure 19 to Figure 22, the fragility surfaces increase sharply to a value of 1.0 as soon as the water height exceeds the height of the pier (7.5 m). This is due to the employed definition of the SLS based on the exceedance of a threshold value of water height. On the other hand, for water height below 7.5 m, the exceedance of the SLS is related to the exceedance of the threshold value of scouring.

Table 8: Probabilities of exceeding the serviceability limit state of the Banija Bridge for different flood scenarios and sizes of debris

No debris						
H \ V	0.2 m/s	0.5 m/s	0.8 m/s	1.2 m/s	1.6 m/s	1.8 m/s
2 m	0	0	0	0	0	0
3 m	0	0	0	0	0	0.025
5 m	0	0	0	0	0.025	0.075
7 m	0	0	0	0	0.075	0.15
>7.5 m	1	1	1	1	1	1
Small-size debris, W_d/H_d = 5 m / 2.1 m						
2 m	0	0	0	0	0	0
3 m	0	0	0.05	0.325	0.625	0.725
5 m	0	0	0.025	0.2	0.625	0.6
7 m	0	0	0	0.175	0.625	0.575
>7.5 m	1	1	1	1	1	1
Medium-size debris, W_d/H_d = 10 m / 2.1 m						
2 m	0	0	0	0	0	0
3 m	0	0.275	0.75	0.95	0.975	1
5 m	0	0.05	0.45	0.8	0.925	0.95
7 m	0	0.025	0.275	0.7	0.875	0.925
>7.5 m	1	1	1	1	1	1
Large-size debris, W_d/H_d = 20 m / 2.1 m						
2 m	0	0	0	0	0	0
3 m	0.3	0.95	1	1	1	1
5 m	0.025	0.75	0.95	1	1	1
7 m	0	0.525	0.875	0.975	1	1
>7.5 m	1	1	1	1	1	1

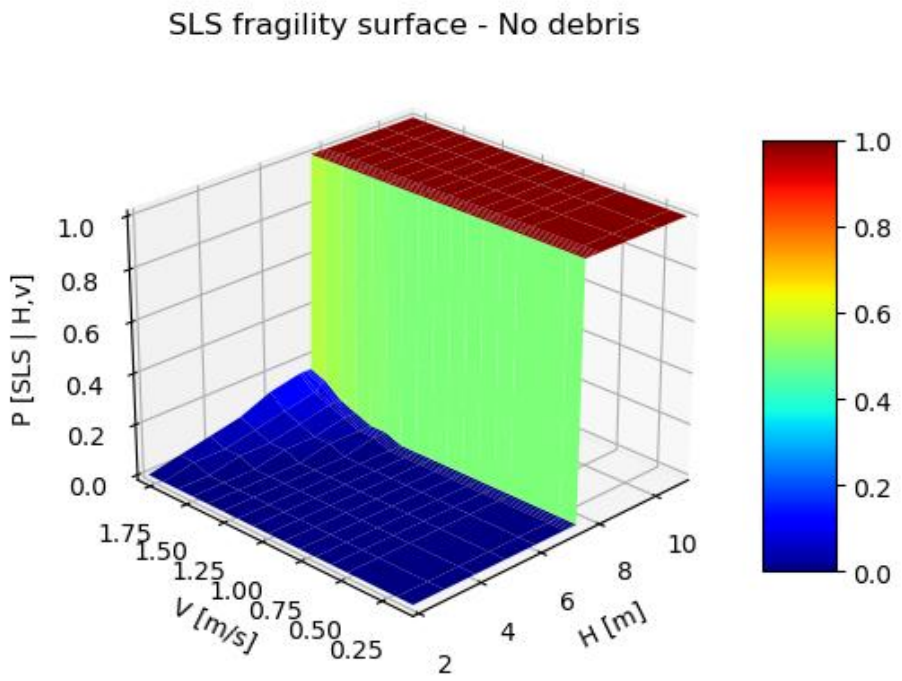

Figure 19: Flood fragility surface of the Banija Bridge for serviceability limit state (No debris scenario).

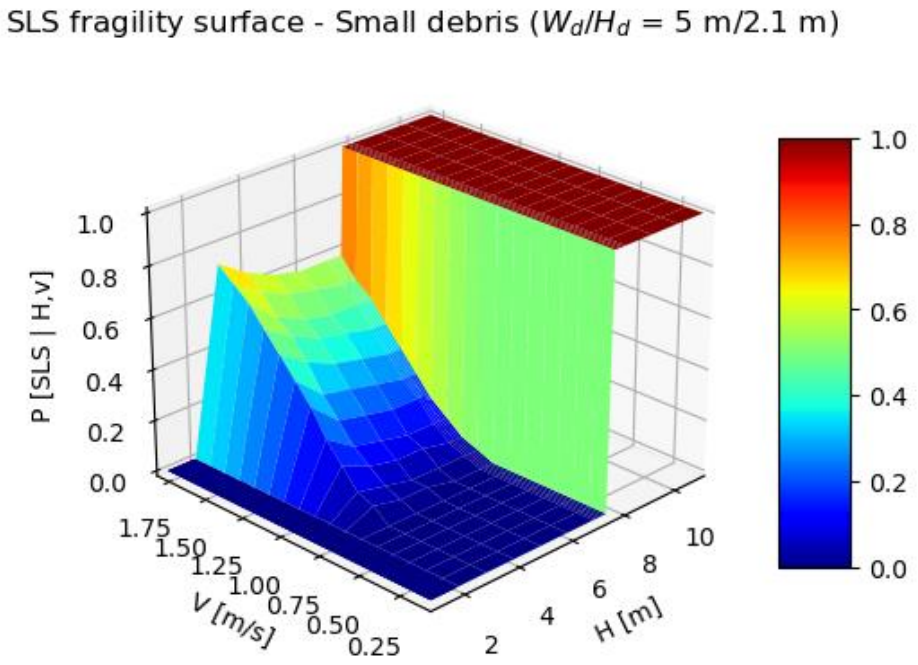

Figure 20: Flood fragility surface of the Banija Bridge for serviceability limit state (Small-size debris accumulation).

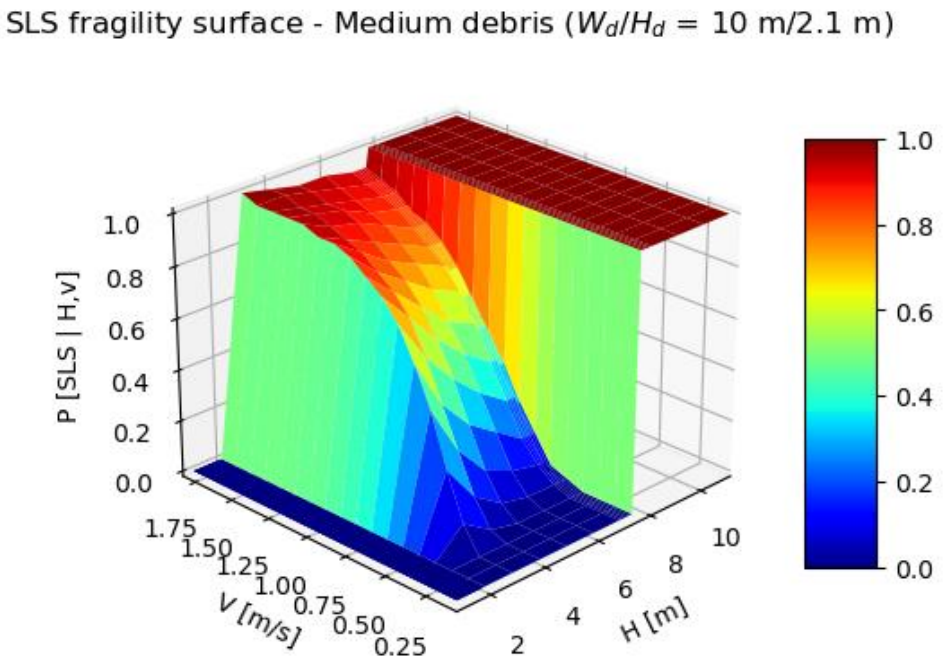

Figure 21: Flood fragility surface of the Banija Bridge for serviceability limit state (Medium-size debris scenario).

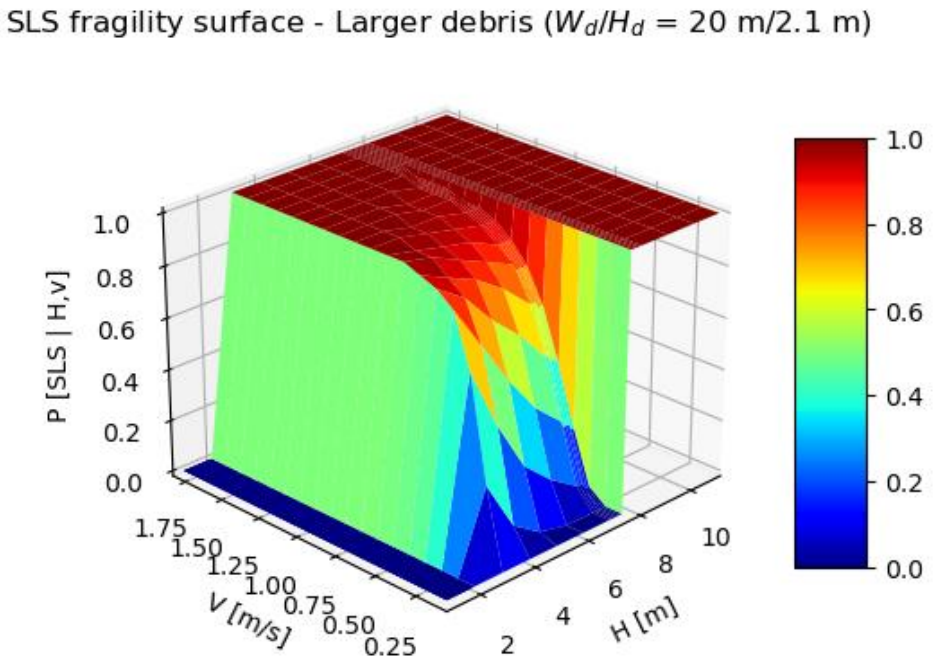

Figure 22: Flood fragility surface of the Banija Bridge for serviceability limit state (Large-size debris scenario).

Debris is shown to affect significantly the probability of exceeding the SLS, which increases in relation to the size of the debris mat. In addition to this, debris is also shown to affect the shape of the fragility surface, with a larger probability of exceeding the SLS being obtained for a lower water height of 3 m (not the highest). This is due to the debris causing larger constriction of the flow at lower water height, which in turn produces a larger increase of water speed, leading to more scour.

The results of Table 8 indicate that the probability of exceeding the SLS in case of no debris is low. The limit state is exceeded only for water height above 7.5 m, which is due to the employed definition of the SLS. In the case of small debris, the likelihood of exceeding the SLS is large only for velocities that are above the upper-bound value from numerical simulations (V =1.2 m/s, see Section 5.3.2). On the other hand, medium and large debris accumulation can lead to a high probability of exceeding the SLS even at lower flow velocities. In the case of medium debris, a high probability of exceeding the SLS is obtained for flow velocities above 0.8 m/s, whereas for large debris, a high probability is reached for flow velocities above 0.5 m/s, irrespectively of the flood height. It should be noted that for water height below 2 m, the accumulation of debris was not considered, which resulted in the probability of exceeding the SLS equal to 0.

Based on the obtained results, monitoring of debris for water height above 3 m is crucial for reliable prediction of the serviceability of the bridge. The performed study also indicated that monitoring of average water speed at the Karlovac measuring station would significantly improve the applicability of the results reported in this deliverable.

7.1.3 Results for ultimate limit state

The results of the analysis were the following fragility surfaces for the ultimate limit state:

- Flood fragility surface for the ultimate limit state (No debris scenario) (Figure 23)
- Flood fragility surface for the ultimate limit state (Large debris, no amplification of scour) (Figure 24)
- Flood fragility surface for the ultimate limit state (Large debris with amplification of scour) (Figure 25)

The ULS fragility surfaces represent the probability of failure of the bridge for a given combination of water height and velocity. A summary of the probabilities of failure for different flood scenarios and two approaches for modelling the effect of debris is presented in Table 9. A colour code is used in the table to ease understanding of the likelihood of failure: i.e. green colour for low likelihood ($P(ULS|H,V) < 0.33$), orange color for medium likelihood ($0.33 \leq P(ULS|H,V) < 0.66$), and red colour for high likelihood ($P(ULS|H,V) \geq 0.66$).

The second and third load scenario differs in the modelling of scour. In the second scenario, debris is considered to apply additional loading on the structure, but the interaction with the scour is neglected. In the third load, the scenario considered the interaction between debris and scour is considered, which results in a larger scour due to constriction of the flow (increase of local flow velocity).

As it can be observed from Figure 23 to Figure 25, the largest probability of failure of the Banija Bridge is obtained for water height submerging the bridge deck (H > 8.2 m) and flow velocities

above 1.2 m. In the scenario with no debris, a high probability of failure is expected only at flow velocities that are already above the upper-bound value from numerical simulations (V > 1.8 m/s). The same conclusion applies for the scenario with large debris (no amplification of scour), but a non-zero probability of failure was obtained at somewhat lower flow velocity (V >1.6 m/s). The reason why failure was only obtained for water heights reaching the deck (H > 8.2 m) is that failure of the bridge was related to the exceedance of the shear capacity of the steel bearings above the middle pier, which required the bridge deck to be submerged.

In the case of the flood loading with amplification of scour due presence of debris, two distinct peaks can be seen on the flood failure surface (see Figure 25). The two peaks are a consequence of two different failure mechanisms which activate in the presence of debris. The peak obtained at water heights below the deck (H < 8.2 m) was found to be a consequence of local scour reaching the base of the foundation, which was conservatively assumed as failure in this study. The second mechanism was, as previously noted, a consequence of the failure of the bearing above the pier. As it can be seen from Figure 25, the amplification of scour due to debris can lead to a non-negligible probability of failure even at flood heights between 2 m and 4 m. However, the flood velocities required to reach a high likelihood of failure are still above the upper-bound velocity from hydraulic simulations (1.2 m/s, see Section 3.4). This conclusion can be most clearly observed from the results of Table 9.

It can be concluded that the failure of the Banija Bridge is expected only for extreme flooding scenarios. However, large debris accumulation can significantly increase the likelihood of failure leading to the potential failure of the bridge even in more likely scenarios. This conclusion highlights the importance of monitoring the debris during flooding. In addition to this, monitoring of average water speed at the Karlovac measuring station would improve the applicability of the results reported in this deliverable.

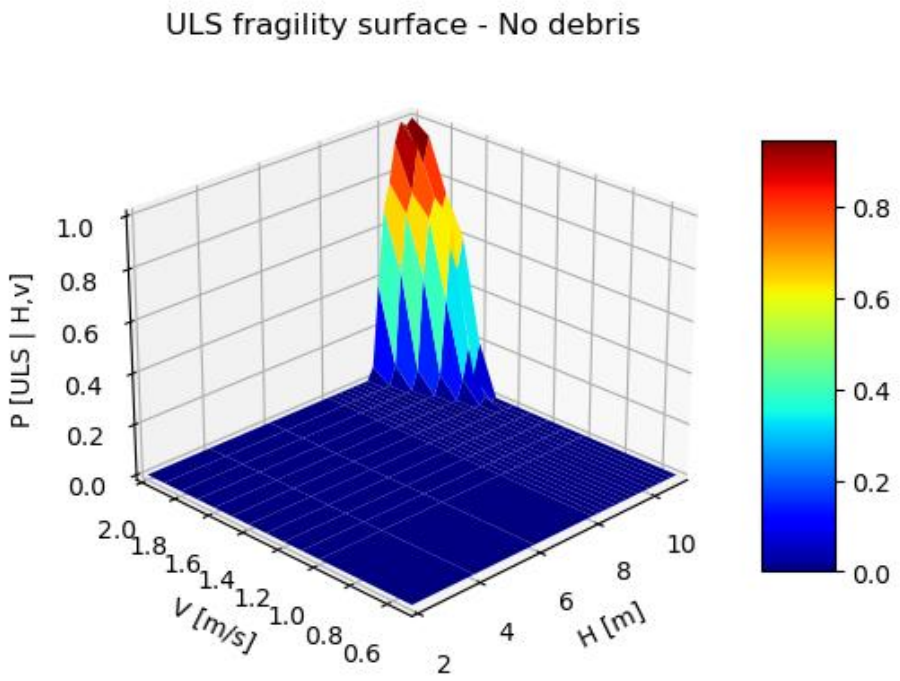

Figure 23: Flood fragility surface of the Banija Bridge for the ultimate limit state (No debris scenario).

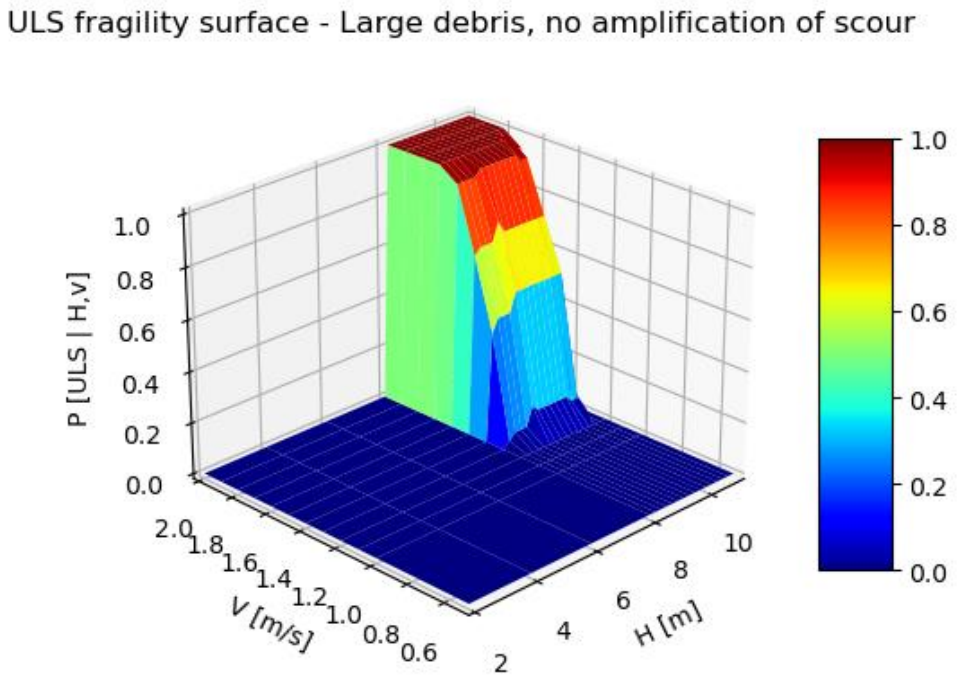

Figure 24: Flood fragility surface of the Banija Bridge for the ultimate limit state (Large debris scenario, no amplification of scour).

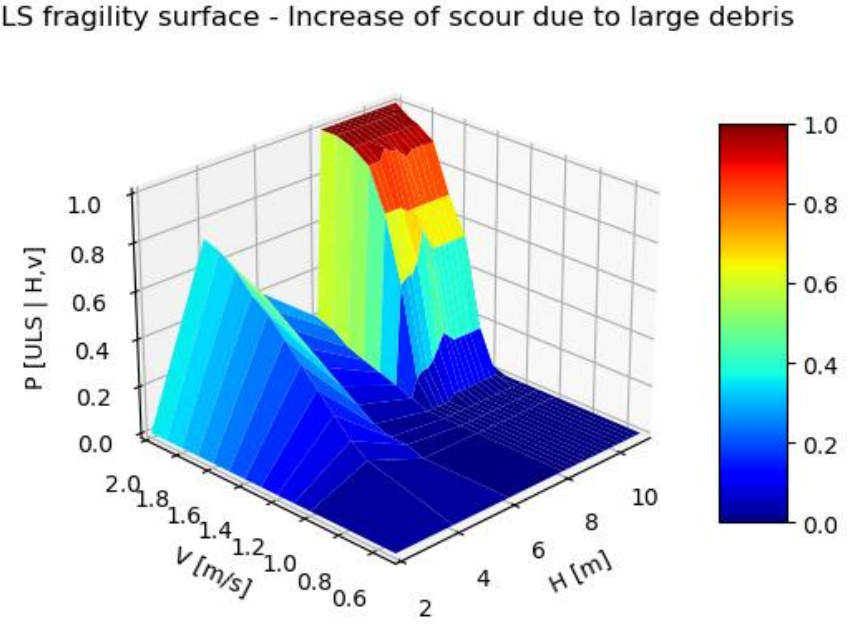

Figure 25: Flood fragility surface of the Banija Bridge for the ultimate limit state (Large debris scenario with amplification of scour).

Table 9: Probabilities of attaining the ultimate limit state of the Banija Bridge for different flood scenarios and two approaches for modelling the effect of debris

No debris						
H \ V	0.5 m/s	1 m/s	1.2 m/s	1.6 m/s	1.8 m/s	2 m/s
2 m	0	0	0	0	0	0
4 m	0	0	0	0	0	0
6 m	0	0	0	0	0	0
8 m	0	0	0	0	0	0
8.2 m	0	0	0	0	0	0
10 m	0	0	0	0	0.075	0.675
Large debris (W_d/H_d = 20 m / 2.1 m), no amplification of scour						
2 m	0	0	0	0	0	0
4 m	0	0	0	0	0	0
6 m	0	0	0	0	0	0
8 m	0	0	0	0	0	0
8.2 m	0	0	0	0.95	1	1
10 m	0	0	0	0.975	1	1
Large debris W_d/H_d = 20 m / 2.1 m with amplification of scour						
2 m	0	0	0	0	0	0
4 m	0	0.1	0.225	0.525	0.65	0.725
6 m	0	0	0.025	0.2	0.3	0.4
8 m	0	0	0	0.075	0.125	0.2
8.2 m	0	0	0	0.75	0.975	1
10 m	0	0	0	0.725	0.975	1

7.2 Karlovac Bridge

7.2.1 Definition of limit states

The serviceability LS of the Karlovac Bridge was defined on exceedance of the scour depth of 3 m (roughly 1/3 the pile length) and water height exceeding 7.5 m, which is 0.5 m below the bridge deck at the lowest part (north part) of the bridge. The selected threshold values are assumed to be the limit value that would require intervention before the safe operation of the bridge can be granted.

The ultimate LS was defined with the failure of the first component. The following failure mechanisms were considered:

- Bending and shear failure at the base of the piers
- Bending failure of the deck at the section above the piers and at the midspan of the bridge
- Failure of the bearing above the piers and at the location of the Gerber hinges (friction mechanism is considered)
- Bearing failure of the foundation (vertical capacity of the piles at the base)

The calculation of the failure mechanism is based on the unfactored capacity of the members. The capacities of reinforced concrete members were computed conservatively without consideration of the contribution of steel reinforcement. This was due to a lack of as build reinforcement drawings, which could be used for the determination of the exact position and distribution of reinforcement. It is expected that the actual failure capacities of the members will be larger than the considered values. It should be noted that if the applied load is below the considered values, it is expected that flooding will not result in structural damage of the main bridge components (damage to the equipment is not excluded).

The bending capacity of the pier was defined based on the section modulus of the pier and the mean tensile strength of concrete C40/50 according to EN-1992-1-1 [7]. The shear strength of the pier was calculated according to equation (6.2.a) from [7] for members without shear reinforcement. The bending capacity of the deck was defined based on section modulus of the deck in the transverse direction and tensile strength of concrete C50/60 according to EN-1992-1-1 [7].

The ultimate capacity of the elastomer bearings above the pier and at the location of the Gerber hinges was based on an ultimate friction criterion. Failure of the bearing is assumed to be attained if the applied load exceeds the maximum friction between the elastomer pad and the concrete surface. The verification is based on the friction coefficient between wet concrete and rubber, which is assumed to amount to 0.50. More precise verification of the deformations of the elastomer bearing was considered to be out-of-the-scour of this study due to the lack of more precise data regarding the dimensions and actual properties of the elastomer bearing.

The failure of the foundation was verified by comparing the applied load to the vertical bearing capacity of the pile base computed according to the Meyerhof method for piles [39].

7.2.2 Results for serviceability limit state

The results of the analysis were the following fragility surfaces for the serviceability limit state:

- Flood fragility surface for serviceability limit state (No debris scenario) (Figure 26)
- Flood fragility surface for serviceability limit state (Small debris scenario) (Figure 27)
- Flood fragility surface for serviceability limit state (Medium debris scenario) (Figure 28)
- Flood fragility surface for serviceability limit state (Large debris scenario) (Figure 29).

A summary of the probabilities of exceeding the SLS for different flood scenarios and sizes of debris is presented in Table 10. A colour code is used in the table to ease understanding of the likelihood of exceeding the serviceability limit state: i.e. green colour for low likelihood ($P(SLS|H,V) < 0.33$), orange color for medium likelihood ($0.33 \leq P(SLS|H,V) < 0.66$), and red colour for high likelihood ($P(SLS|H,V) \geq 0.66$).

The obtained results are similar to the results obtained for the Banija Bridge. As it can be seen from Figure 26 to Figure 29, the fragility surfaces increase sharply to a value of 1.0 as soon as the water height exceeds the threshold value of 7.5 m. On the other hand, for water height below 7.5 m, the exceedance of SLS is related to the exceedance of the threshold value of scour. Non-zero probabilities of exceeding the SLS are obtained only for water height above 5 m. Compared to the results obtained for the Banija Bridge, the SLS is obtained at larger water levels. This is due to the foundation being located (at the lower part) about 2.2 m above the zero-mark water level, which is higher than the elevation of the Banija's Bridge foundation. Additionally, debris was assumed to be presented on the bridge only if water height above the foundation level was higher than the assumed depth of the debris (2.1 m), which means that the minimal water height after which debris are considered amounts to 4.3 m.

Debris is shown to affect significantly the probability of exceeding the serviceability limit, which increases in relation to the size of the debris mat. Monitoring of debris can thus be crucial for precise estimation of the bridge limit state.

Debris is also shown to affect the shape of the fragility surface, with a larger probability of exceeding the SLS being obtained for a lower water height of 5 m (not the highest water level). This is due to the debris causing larger constriction of the flow at lower water height, which in turn produces a larger increase of water speed, leading to more scour.

The results of Table 10 indicate that the probability of exceeding the SLS in case of no debris is low. The limit state is exceeded only for water height above 7.5 m, which is due to the employed definition of the SLS. In the case of small debris, the likelihood of exceeding the SLS is large only for velocities that are above the upper-bound value from numerical simulations (V =1.2 m/s, see Section 3.4). On the other hand, medium and large debris accumulation can lead to a high probability of exceeding the SLS even at lower flow velocities. In the case of medium debris, a high probability of exceeding the SLS is obtained for flow velocities above 0.8 m/s, whereas for large debris, a high probability is reached for flow velocities above 0.5 m/s.

Table 10: Probabilities of exceeding the serviceability limit state of the Karlovac Bridge for different flood scenarios and sizes of debris

No debris						
H \ V	0.2 m/s	0.5 m/s	0.8 m/s	1.2 m/s	1.6 m/s	1.8 m/s
2 m	0	0	0	0	0	0
3 m	0	0	0	0	0	0
5 m	0	0	0	0	0	0
7 m	0	0	0	0	0	0
>7.5 m	1	1	1	1	1	1
Small-size debris, W_d/H_d = 5 m / 2.1 m						
2 m	0	0	0	0	0	0
3 m	0	0	0	0	0	0
5 m	0	0	0.05	0.325	0.625	0.725
7 m	0	0	0	0.075	0.3	0.425
>7.5 m	1	1	1	1	1	1
Medium-size debris, W_d/H_d = 10 m / 2.1 m						
2 m	0	0	0	0	0	0
3 m	0	0	0	0	0	0
5 m	0	0.4	0.825	0.95	1	1
7 m	0	0.05	0.4	0.8	0.925	0.95
>7.5 m	1	1	1	1	1	1
Large-size debris, W_d/H_d = 20 m / 2.1 m						
2 m	0	0	0	0	0	0
3 m	0	0	0	0	0	0
5 m	0.475	0.975	1	1	1	1
7 m	0.05	0.8	0.975	1	1	1
>7.5 m	1	1	1	1	1	1

Based on the obtained results, monitoring of debris for water height above 4 m is crucial for reliable prediction of the serviceability of the bridge. The performed study also indicated that monitoring of average water speed at the Karlovac measuring station would improve significantly the applicability of the results reported in this deliverable.

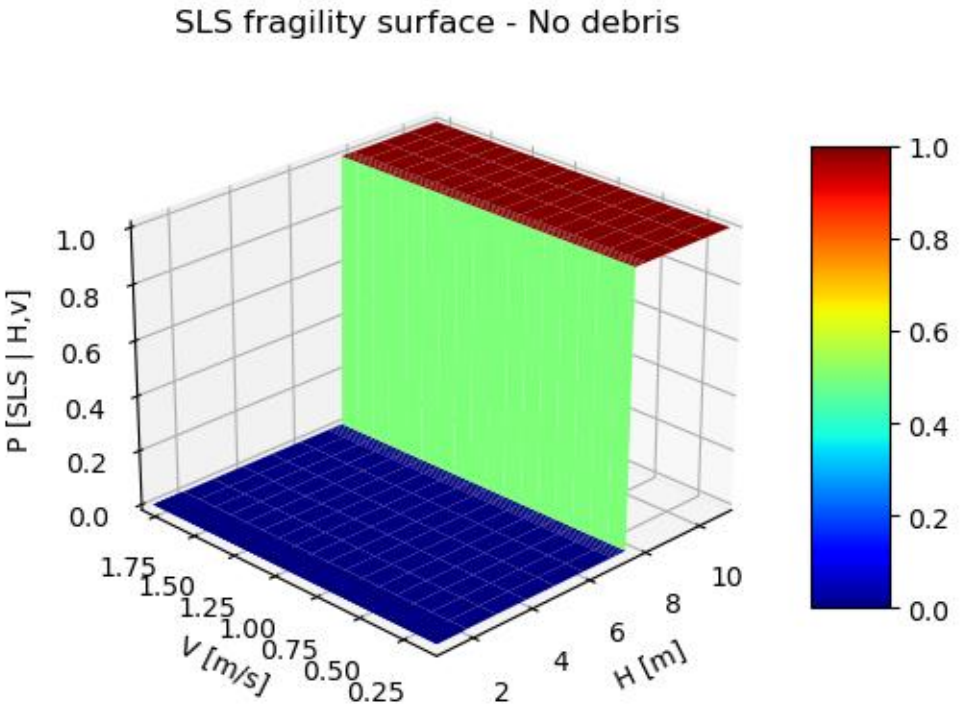

Figure 26: Flood fragility surface of the Karlovac Bridge for serviceability limit state (No debris scenario).

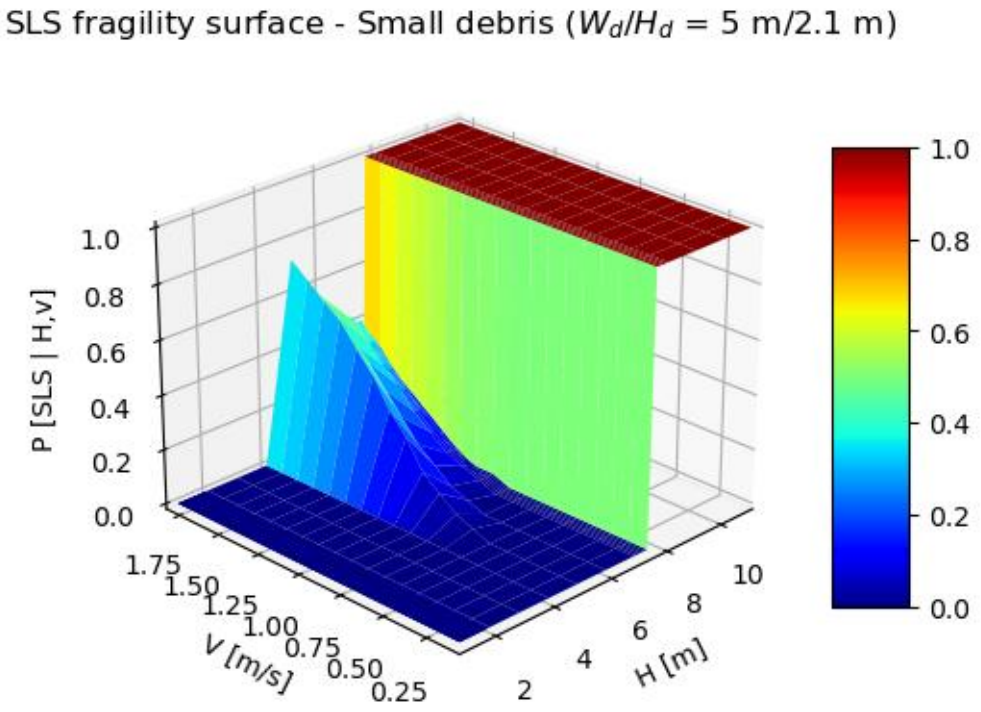

Figure 27: Flood fragility surface of the Karlovac Bridge for serviceability limit state (Small-size debris accumulation).

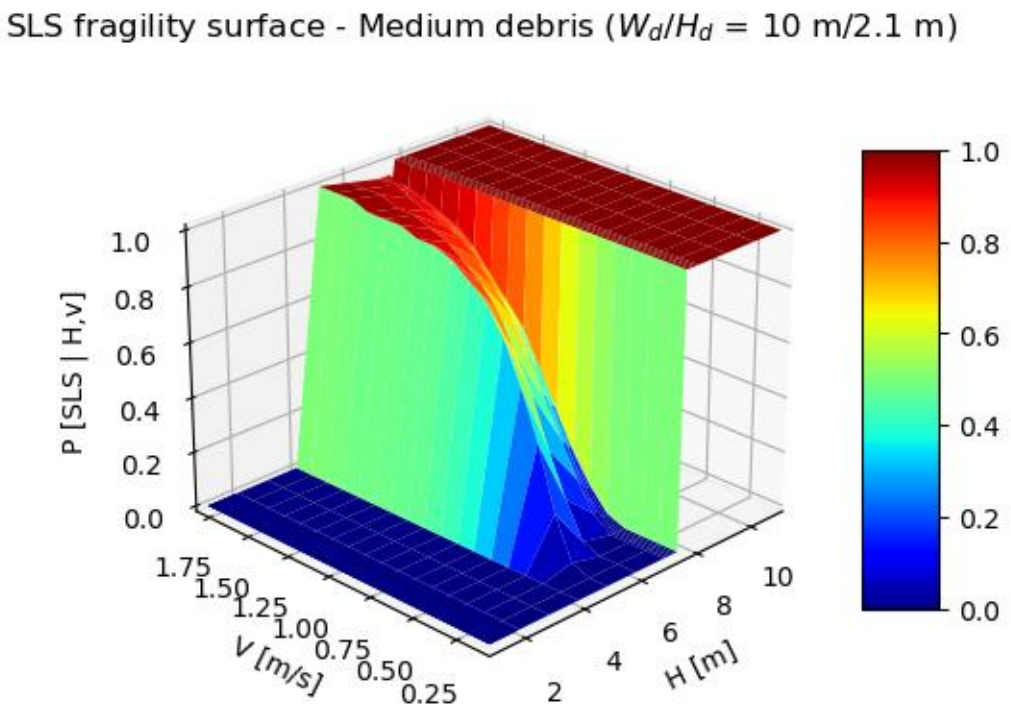

Figure 28: Flood fragility surface of the Karlovac Bridge for serviceability limit state (Medium-size debris accumulation).

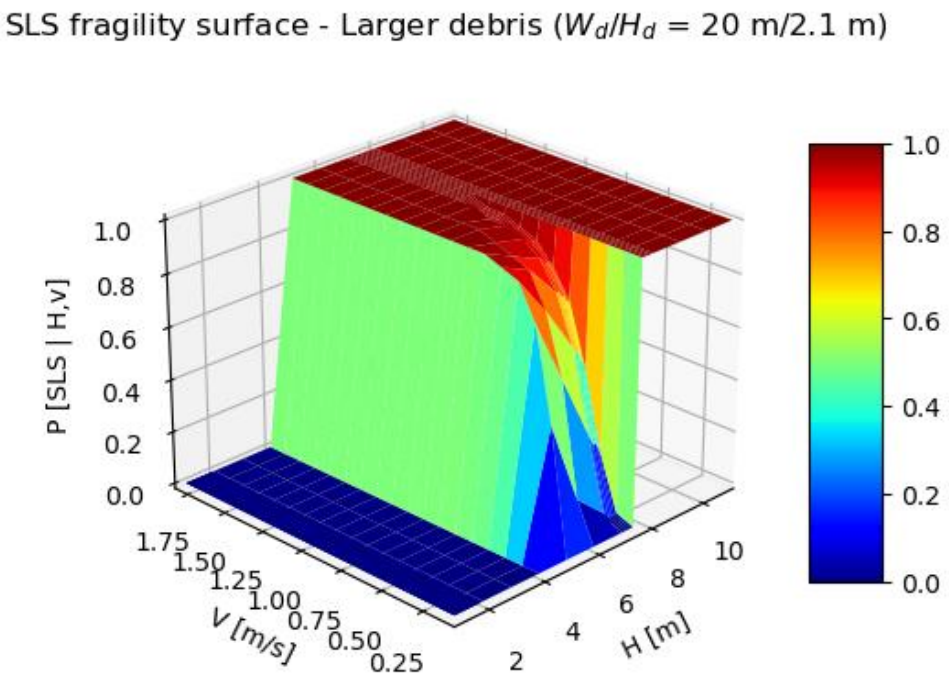

Figure 29: Flood fragility surface of the Karlovac Bridge for serviceability limit state (Large-size debris accumulation).

7.2.3 Results for ultimate limit state

A preliminary study of the ultimate limit state of the Karlovac Bridge, which is documented herein, indicated that the failure of the bridge due to flood loading is not expected. As a result, it was decided not to undertake a rigorous vulnerability analysis. An additional reason is the lack of data regarding the construction materials and disposition of reinforcement, which limit the precision of such analysis significantly. Instead, this section documents the results of the primary (deterministic) flood analysis, which was used to reach such a conclusion.

Table 11 presents the total horizontal and vertical flood-load action on the Karlovac Bridge for different water heights and velocities. The presented results consider the scenario with large debris accumulation and amplification of scour due to debris, which was found to produce the largest actions among all other scenarios.

As it can be seen from *Table* 11, the flood loading increases with both water height and flow velocity. For a water height of 2 m, the loading is zero because the water is still below the foundation level of the bridge. The most severe increase of the flood loading is obtained when the water level reaches the deck (H > 8 m). This is because the deck starts to be affected by hydrodynamic and debris pressure. In addition, the bridge deck starts to be loaded by the combined action of hydrodynamic uplift and buoyancy forces, which results in a vertical uplift action on the bridge.

The most severe flooding scenario is obtained considering the upper bound flood velocity of 1.2 m/s and water height of 10 m. At the height of 12 m, the bridge is entirely submerged, which results in a lower drag coefficient for the deck and a lower flow velocity compared to the surface level of the flow (flow velocity is the largest at the surface).

Table 11: Total horizontal and vertical flood-load action on the Karlovac Bridge for different water heights and velocities (scenario with debris and amplification of scour due to debris)

H	V	Ry [kN]	Rz [kN]
2 m	0.50 m/s	0	0
	0.85 m/s	0	0
	1.20 m/s	0	0
4 m	0.50 m/s	45	0
	0.85 m/s	134	0
	1.20 m/s	275	0
8 m	0.50 m/s	159	712
	0.85 m/s	461	1484
	1.20 m/s	919	2657
10 m	0.50 m/s	158	7211
	0.85 m/s	457	7983
	1.20 m/s	913	9156
12 m	0.50 m/s	158	20671
	0.85 m/s	456	20778
	1.20 m/s	910	20941

Due to the pile foundation system, the bridge is also less vulnerable to scour related failure. The worst-case scenario analysis with amplification of scour due to debris also indicated that scour would never reach the base of the foundation.

Table 12 presents a summary of the failure utilization percentages (UP) of the Karlovac Bridge members. The results were obtained considering different water heights, a constant (upper-bound) flow velocity of 1.2 m/s, and the flood-loading scenario with debris and amplification of scour due to debris. A value of 100% indicates that the failure of a particular bridge member is reached.

Table 12: Failure utilization percentages for the Karlovac Bridge members for the different water heights (flow velocity 1.2 m/s) and the scenario with debris and scour

H \ UP [%]	Column bending	Column shear	Deck bending (above pier)	Deck bending (midspan)	Column bearing	Gerber bearing
4 m	0.1	1.9	0.1	0.2	0.5	0.0
8 m	0.1	0.3	0.4	2.0	0.1	3.8
10 m	0.2	0.6	0.4	2.0	0.3	4.5
12 m	0.3	0.8	0.4	2.0	0.5	6.4

As it can be seen from Table 12, the failure utilization percentages of the bridge members are relatively low. The largest value (6.4%) was obtained for the Gerber hinge. The utilization percentages for other failure mechanisms were even lower. Failure due to exceedance of the bearing capacity was also disregarded based on a comparison of worst-case action to the bearing capacity at the pile tip.

Since all utilization percentages are below 100%, the failure of the bridge is not expected. It should be further noted that the actual failure loads are likely to be significantly larger because the contribution of reinforcement was neglected in the calculation. Due to the conservative definition of the failure loads, it is actually expected that the bridge will be able to sustain flooding loads without structural damage to the main bridge components. However, this conclusion may not hold true for the equipment of the bridge, which was not considered within this study. Additionally, the analysis did not consider the poor condition state of the bridge outlined in deliverable D3.2 [5] (especially of the Gerber hinge, which is the most critical component of the bridge). As a result, the conclusion reached in this deliverable should be treated with caution. The authors recommend additional safety assessment and rehabilitation of the bridge.

8 Conclusions

This deliverable addressed the vulnerability assessment of the two case study bridges, i.e. Banija Bridge and Karlovac Bridge. The major outcome of the deliverable are fragility surfaces for the serviceability and ultimate limit states (SLS and ULS), which represent the probability of exceeding the designated limit states for a given combination of water height and water flow velocity. These results represent the input data for the following project activities and are crucial for the development of the risk forecasting tool within WP5 and validation activities within WP6.

The SLS for the two bridges was defined based on the exceedance of selected threshold values for the scour depth and water height. The selected threshold values are assumed to be a limit value that, if exceeded, no longer provide safe operation of the bridge. In such a case, the bridge needs to be closed for traffic, which can affect the evacuation routes. The fragility surfaces were presented in both a summary table and graphical form. A colour-coding scheme was introduced to facilitate the interpretation of the results, i.e. green colour for low likelihood ($P(SLS|H,V) < 0.33$), orange colour for medium likelihood ($0.33 \leq P(SLS|H,V) < 0.66$), and red colour for high likelihood ($P(SLS|H,V) \geq 0.66$) of exceedance of the SLS. These results will be integrated into the GIS maps of the city of Karlovac and linked to the real-time data of water height measurements.

The results of the analyses indicate that the SLS of the bridges is affected significantly by the accumulation of debris, which constricts the flow of the water, which leads to an amplification of scour due to the local increase of the flow velocity. As a result, the fragility surfaces for the SLS were obtained considering several sizes (quantities) of debris accumulation (no debris, small-size, medium-size and large-size debris accumulation). The appropriate fragility surface should be selected based on the presence and size of debris. The monitoring of debris was thus found to be an important parameter for the prediction of the serviceability of the case study bridges.

The ULS of the case study bridges was also examined. The failure of the bridge was defined based on the failure of the first component, considering no safety factors in capacities. Several failure mechanisms were considered, such as bending or shear failure of the piers, bending failure of the deck, shear failure of the bearings and failure of the foundations due to exceedance of the bearing capacity. The level of detail in the definition of the failure capacity depended on the availability of data. In the case of Karlovac Bridge, the failure capacities of the pier and the deck were defined without consideration of the contribution of reinforcement, which was a consequence of the lack of a construction plan that could be used for the definition of the material properties and distribution of reinforcement. As a result, the level of detail of the analyses performed for the Banija and the Karlovac Bridge also differed.

In the case of the Banija Bridge, a fully probabilistic vulnerability analysis was performed. The results of the analysis were three fragility surfaces for different modelling assumptions regarding scour and debris. The fragility surfaces were presented in both a summary table and graphical form. On the other hand, in the case of the Karlovac Bridge, only a deterministic flood analysis was performed because it was concluded that failure due to severe flooding is not expected. An additional reason was the lack of data regarding the construction materials as well as location and amount of reinforcement, which would significantly limit the precision of such analyses.

The vulnerability analysis of the Banija Bridge indicated that failure of the bridge is expected only for extreme flooding scenarios. However, large debris accumulation can significantly increase the likelihood of failure leading to the potential failure of the bridge even in more likely scenarios. Two failure mechanisms were identified. The first failure mechanism of the Banija Bridge is related to the failure of the steel bearing above the pier. Such a failure mechanism is triggered when the deck is partly or fully submerged. The second failure mechanism is related to the undermining of the foundation due to extreme scour. Such a failure mechanism can be triggered by a large accumulation of debris, even at water levels significantly below the bridge deck.

In the case of the Karlovac Bridge, the results of a deterministic flood analysis indicated a quite low failure utilization percentage of the bridge members, despite considering a very conservative definition of the failure loads (reinforcement neglected). Accumulation of large debris and scour was found to contribute significantly to the flooding loading. Despite this, the study indicates that the bridge could sustain the flood loading without structural damage. It should be noted, however, that this conclusion does not consider the damage of the equipment, which was out-of-the-scope of the analysis. Additionally, the analysis did not consider the poor condition state of the bridge outlined in deliverable D3.2 [3] (especially of the Gerber hinge, which is the most critical component of the bridge). As a result, the conclusion reached in this deliverable should be treated with caution.

A similar caveat also applies to the Banija Bridge. The authors recommend reliability analysis and rehabilitation of both studied bridges. Critical issues that need special attention were highlighted in deliverable D3.2 [3].

The final remark of this deliverable is that the definition of the limit state of the case study bridges could be improved significantly by establishing a monitoring system for debris accumulation. In addition, monitoring of average water velocity at the Karlovac measuring station would significantly improve the applicability of the results reported in this deliverable. Based on the Deliverable 2.2 (ref) for prediction of changes of water flow and water level of the Kupa River at Karlovac case study area showed that climate change is likely to impact future flows and water levels of the Kupa River. Although the changes in annual average flows and water levels are expected to be small and not significant, models predict a significant increase in flow and water level in winter months and its decrease in summer months for both moderate and extreme scenarios, with bigger changes in the extreme scenario, especially in the period from 2041 to 2070. For that period, a significant decrease in water flow and level is also expected in the autumn months for the extreme scenario. In the moderate scenario, an increase in the frequency of flood events is not expected, whereas, in the extreme scenario, there is an indication of an increase in the frequency of small and moderate floods and a decrease in the frequency of large floods (100 to 1000 years return period). Therefore the establishment of a monitoring system and improvement of the bridge condition is strongly recommended.

9 References

[1] M. Burić and S. Grgurić, "oVERFLOw Deliverable D2.2: Climate downscaling and flooding scenarios for selected area," 2021.

[2] S. Skarić Palić and I. Stipanović, "oVERFLOw Deliverable D2.1: Database of historical flood events in selected areas," 2020.

[3] Ascon institut d.o.o, "Retrofitting of the Banija Bridge - The old bridge over the Kupa River in Karlovac," 2017.

[4] Ascon institut d.o.o, "Report on in-situ investigations of the Banija Bridge - The old bridge over Kupa River in Karlovac," 2017.

[5] A. Kosič, Mirko; Hekič, Doron; Kalin, Jan; Anžlin, "oVERFLOw Deliverable 3.2: Report on investigation works and monitoring of bridges," 2021.

[6] CEN, "European standard EN 1993-1-1:2005. Eurodoce 3: Design of steel structures - Part 1-1: General rules and rules for buildings," European Committee for Standardization, Brussels, 2005.

[7] CEN, "European standard EN 1992-1-1:2004. Eurocode 2: Design of concrete structures - Part 1-1: General rules and rules for buildings," European Committee for Standardization, Brussels, 2004.

[8] Geoexpert IGM, "Report on the principal inspection of the Karlovac Bridge – Reg.br. HRMOS/BCP-435," Zagreb, Croatia, 2020.

[9] R. B. Terzaghi, Karl ; Peck, *Soil Mechanics in Engineering Practice, 2rd Edition*. New York: John Wiley and Sons, 1967.

[10] M. Hatanaka and A. Uchida, "Empirical Correlation Between Penetration Resistance and Internal Friction Angle of Sandy Soils," *Soils Found.*, vol. 36, no. 4, pp. 1–9, 1996, doi: https://doi.org/10.3208/sandf.36.4_1.

[11] N. Janbu, "Sediment deformations," Bulletin 3., University of Trondheim, Norwegian University of Science and Technology, 1998, p. 86.

[12] B. H. Fellenius, *Basics of Foundation Design*, no. November. Electronic Edition (www.Fellenius.net), 2009.

[13] D. Kolarić and Ž. Tusić, "Flood Protection System of the City of Karlovac – Sensitivity of the Input Parameters," in *7th Croatian Water Conference with International Partecipationcipation*, 2019, pp. 723–732.

[14] M. Vořechovský and D. Novák, "Correlation control in small-sample Monte Carlo type simulations I: A simulated annealing approach," *Probabilistic Eng. Mech.*, vol. 24, no. 3, pp. 452–462, 2009, doi: https://doi.org/10.1016/j.probengmech.2009.01.004.

[15] M. Dolsek, "Incremental dynamic analysis with consideration of modeling uncertainties," *Earthq. Eng. \& Struct. Dyn.*, vol. 38, no. 6, pp. 805–825, 2009, doi: https://doi.org/10.1002/eqe.869.

[16] R. E. Melchers, *Structural Reliability Analysis and Prediction*. Wiley, 1999.

[17] JCSS, "Probabilistic model code, Part 3, Resistance models, Section 3.0, Static Properties of

Structural Steel," 2001. [Online]. Available: https://www.jcss-lc.org/publications/jcsspmc/part_iii.pdf.

[18] B. Aygün, L. Dueñas-Osorio, and R. Padgett, Jamie E.; DesRoches, "Efficient Longitudinal Seismic Fragility Assessment of a Multispan Continuous Steel Bridge on Liquefiable Soils," *J. Bridg. Eng.*, vol. 16, no. 1, pp. 93–107, 2011.

[19] Y. Zhang, "PROBABILISTIC STRUCTURAL SEISMIC PERFORMANCE ASSESSMENT METHODOLOGY AND APPLICATION TO AN ACTUAL BRIDGE-FOUNDATION-GROUND SYSTEM," UNIVERSITY OF CALIFORNIA, SAN DIEGO, 2006.

[20] I. M. Boulanger, Ross W.; Idriss, "Probabilistic Standard Penetration Test–Based Liquefaction–Triggering Procedure," *J. Geotech. Geoenvironmental Eng.*, vol. 138, no. 10, pp. 1185–1195, 2012.

[21] H. Kim, S.-H. Sim, J. Lee, Y.-J. Lee, and J.-M. Kim, "Flood fragility analysis for bridges with multiple failure modes," *Adv. Mech. Eng.*, vol. 9, no. 3, p. 1687814017696415, 2017.

[22] P. A. . Johnson, P. E. . Clopper, L. W. . Zevenbergen, and P. F. . Lagasse, "Quantifying Uncertainty and Reliability in Bridge Scour Estimations," *J. Hydraul. Eng.*, vol. 141, no. 7, 2015.

[23] M. Zhu, "The OpenSeesPy Library, Version 3.2.2 – 2020.," 2020. https://openseespydoc.readthedocs.io/.

[24] "Open system for earthquake engineering simulation (OpenSees)," *Pacific Earthquake Engineering Research Center, University of California, Berkeley, CA.*, 2020. https://opensees.berkeley.edu.

[25] "CSI SAP2000 v.23 - Structural analysis and design software," *Computer & Structures, inc.*, 2021. https://www.csiamerica.com/products/sap2000.

[26] W. F. Van Impe and S.-T. Wang, "The advanced p-y method for analyzing the behaviour of large-diameter monopiles supporting offshore wind turbines," *E3S Web Conf.*, vol. 205, p. 12008, 2020, doi: 10.1051/e3sconf/202020512008.

[27] "OpenSeesWiki - PySimple 1 Material." https://opensees.berkeley.edu/wiki/index.php/PySimple1_Material.

[28] "OpenSeesWiki - TzSimple1 Material." https://opensees.berkeley.edu/wiki/index.php/TzSimple1_Material.

[29] "OpenSeesWiki - QzSimple 1 Material." https://opensees.berkeley.edu/wiki/index.php/QzSimple1_Material.

[30] "OpenSeesWiki - ElasticPP Material." https://opensees.berkeley.edu/wiki/index.php/Elastic-Perfectly_Plastic_Material.

[31] API, "Recommended Practice for Planning, Designing and Constructing Fixed Offshore Platforms—Working Stress Design," Washington, D.C., 2003.

[32] L. C. Reese and W. F. Van Impe, *Single Piles and Pile Groups Under Lateral Loading - 2nd Edition*, 2nd Editio. CRC Press, Taylor & Francis Group, 2011.

[33] A. Pais and E. Kausel, "Approximate formulas for dynamic stiffnesses of rigid foundations," *Soil Dyn. Earthq. Eng.*, vol. 7, no. 4, pp. 213–227, 1988, doi: https://doi.org/10.1016/S0267-7261(88)80005-8.

[34] R. Mosher, "Load-transfer Criteria for Numerical Analysis of Axially Loaded Piles in Sand," Vicksburg, Mississippi, 1984.

[35] API, "Recommended Practice for Planning, Designing and Constructing Fixed Offshore Platforms — Working Stress Design," Washington, D.C., 2005.

[36] V. N. Vijayvergiya, "Load-movement characteristics of piles," in *4th Annual Symposium of the Waterway, Port, Coastal, and Ocean Division*, 1977, pp. 1256–1266.

[37] G. G. Meyerhof, "Some Recent Research on the Bearing Capacity of Foundations," *Can. Geotech. J.*, vol. 1, no. 1, pp. 16–26, 1963, doi: 10.1139/t63-003.

[38] J. B. Burland and M. C. Burbidge, "Settlement of Foundations on Sand and Gravel.," *Proc. Inst. Civ. Eng.*, vol. 78, pp. 1325–1381, 1985, doi: 10.1680/iicep.1985.1058.

[39] G. G. Meyerhof, "Bearing Capacity and Settlement of Pile Foundations," *J. Geotech. Eng. Div.*, vol. 102, no. 3, pp. 197–228, 1976, doi: 10.1061/AJGEB6.0000243.

[40] Standards Australia, "Australian Standard AS-5100.2-2004. Bridge design - Part 2: Design loads.," Sydney, Australia, 2004.

[41] T. Ahamed, J. G. Duan, and H. Jo, "Flood-fragility analysis of instream bridges – consideration of flow hydraulics, geotechnical uncertainties, and variable scour depth," *Struct. Infrastruct. Eng.*, vol. 17, no. 11, pp. 1494–1507, 2021, doi: 10.1080/15732479.2020.1815226.

[42] L. A. Arneson, L. W. Zevenbergen, P. F. Lagasse, and P. E. Clopper, "Evaluating Scour at Bridges. HEC-18. Fifth Edition, Hydraulic Engineering Circular No. 18. Publication," 2012.

[43] P. F. Lagasse, L. W. Zevenbergen, and P. E. Clopper, "Effects of debris on bridge pier scour," in *Proceedings 5th International Conference on Scour and Erosion (ICSE-5)*, 2010, pp. 854–863, [Online]. Available: https://henry.baw.de/handle/20.500.11970/100218.